Predicting the Phase Behavior of Polymer Systems with the GC-SAFT-VR Approach

Yun Peng,[†] Kimberly D. Goff,[†] M. Carolina dos Ramos,[†] and Clare McCabe*[,†,‡]

Departments of Chemical and Biomolecular Engineering and Chemistry, Vanderbilt University, Nashville, Tennessee 37215-1604

The recently developed heteronuclear group contribution SAFT-VR equation (GC-SAFT-VR) [Peng et al. *Fluid Phase Equilib.* 2009, *227* (2), 131−144] enables the predictive study of the thermodynamic properties of fluids and their mixtures by using a molecular-based model in which the molecules are described by heterosegmented chains in which each type of segment represents a functional group present in the molecule. Given the success of the GC-SAFT-VR approach in predicting the fluid phase equilibria of mixtures without fitting to any mixture data, and the known difficulties in determining equation-of-state parameters for polymers because of the lack of coexistance data, in this work, we extend the GC-SAFT-VR equation to study the phase equilibria of small molecules in polymer systems. The results demonstrate the ability of the GC-SAFT-VR equation of state to predict the vapor−liquid and liquid−liquid equilibria of polymer solutions and accurately capture the effects of polymer molecular weight and molecular topology on phase behavior.

Introduction

Understanding vapor−liquid equilibrium (VLE) and liquid−liquid phase equilibrium (LLE) is very important to polymer production, as polymers are generally synthesized in one- or two-phase systems with a mixture of solvents, unreacted monomers, and additives that must be separated[1] from the product. Knowledge of the phase behavior of polymer systems is therefore very important in the design and optimization of polymerization reactors, in which control of the phase behavior is essential in order to either avoid or induce a phase transition, as well as separation and devolatilization equipment. In the latter, the remaining monomer must be removed from the polymer product under low-pressure and high-temperature conditions to ensure product purity and to reduce the environmental and health and safety hazards related to producing and using polymers.[2]

Although a large body of experimental data is available on the phase behavior of polymer systems, experiments involving high pressure and/or components at supercritical conditions can be difficult and expensive to perform. Hence, it is of great interest to study the thermodynamic properties of polymer systems using an efficient and robust theoretical modeling tool that can be used to predict phase behavior in regions of the phase diagram where experimental measurements are not available. To this end, a number of thermodynamic models have been proposed in the literature to describe the phase behavior of polymer systems, such as activity coefficient models and equations of state. Whereas traditional equations of state, such as cubic equations, usually work well for simple, nearly spherical molecules, such as small alkanes, nitrogen, and carbon monoxide, they tend to give poor predictions for polymer systems,[3] because they have not been derived from a theoretical basis that accommodates the complexity of molecular shape. More recently, significant efforts have been focused on developing molecular-based equations of state to model polymers.[4] Of these, we focus on the statistical associating fluid theory (SAFT),[5,6] in which molecules are described as chains of tangentially bonded spherical segments. The SAFT approach, in its many variations, has been successfully applied to study the thermodynamics and phase behavior of a wide range of fluids and their mixtures (see, for example, the excellent reviews of Müller and Gubbins[7,8] and Economou[3]). Given the underlying molecular model in SAFT, its application to polymeric fluids is a natural extension, as a polymer can simply be described as a very long chain of tangentially bonded spherical segments; for example, polyethylene (PE) can been modeled as a very long *n*-alkane chain.[7]

Several versions of the SAFT equation of state (EOS) have been applied to describe the phase behavior of polymer[9−32] and copolymer systems.[33−43] In particular, Huang and Radosz proposed an engineering version of the original SAFT EOS (HR-SAFT)[9,44] that has been applied to a wide range of polymers and, in particular, polyolefin systems.[11−13,45] More recently, Sadowski et al.[46,47] developed the perturbed-chain SAFT (PC-SAFT) equation which has been shown to provide excellent results in the description of VLE and LLE for a wide range of polymer systems.[16−21,26,28−31,42,48] At a similar level of theory, the SAFT-VR approach proposed by Gil-Villegas et al.[49,50] has been successfully applied to study the phase behavior of a wide range of systems,[51−82] including the absorption of light hydrocarbons in polyethylene[22,24,83] and the cloud-point curves of polyethylene solutions.[23]

One of the issues when modeling polymer systems is characterizing branching (i.e., side chains on the backbone) and heterogeneity (e.g., functional groups of different molecular composition) in the polymer structure. To better describe the topology of polymers, such as different functional groups within the repeat unit and polymers that have side chains or pendant groups, heterosegmented versions of SAFT that allow the model chain to be composed of segments of different size and/or energy have been proposed by several authors.[25,34,37,38,84] Typically, in these heteronuclear approaches, copolymers are described by two distinct types of segments, the ratio of which is described in a statistical fashion through segment and bonding fractions that are estimated from the known molecular structure, such as the NMR-derived branch density and the mass fraction of comonomers in the copolymer composition.[34]

One of the challenges in modeling polymer systems is determining the model parameters. In SAFT, as in many equations of state, pure-component parameters are generally

* To whom correspondence should be addressed. Tel.: 615 322 6853. Fax: 615 3437951. E-mail: c.mccabe@vanderbilt.edu.
[†] Department of Chemical and Biomolecular Engineering.
[‡] Department of Chemistry.

10.1021/ie900795x
Published on Web 12/15/2009

determined by regressing experimental vapor pressure and saturated liquid density data. Identifying pure-component parameters for a polymer is more difficult, and afflicted with a higher degree of uncertainty compared to the case of volatile substances,[18] as coexistence data are not available. As an alternative, pure-polymer parameters are often calculated by fitting to *PVT* data; however, it has been shown that SAFT parameters for the dispersion energy and segment size obtained from *PVT* data do not work well when applied to the description of mixture phase behavior, even when large binary interaction parameters are used.[3] Alternatively, polymer parameters can be regressed from correlations based on the parameters for smaller molecules in a homologous series. This approach works well for polyolefins by extrapolation of *n*-alkane parameters to high molecular weights,[22,27,85] but has been shown to fail for other types of polymers because the effects of other functional groups in the polymer repeat unit are not properly taken into account.[127]

To overcome these parameter determination issues, several approaches[34,38,84] have been proposed to obtain parameters for different types of polymers within a heterosegmented SAFT model. For example, in the copolymer-SAFT approach proposed by Banaszak et al.,[34] the parameters for backbone and branch segments in a branched polymer are obtained from the parameter regression for polyethylene and the branch-corresponding alkane, respectively; however, this approach requires the use of a temperature-dependent binary interaction parameter between each segment type in the polymer molecule and the solvent that is obtained by fitting to PE/alkane mixture data. Subsequently, Gross and co-workers[38] proposed the poly(α-*co*-β) model, based on the work of Banaszak et al.,[34] to study copolymers using the PC-SAFT equation. In this approach, the parameters for the comonomer segments α and β are regressed from experimental data for the corresponding homopolymer + solvent phase equilibrium, and three correction parameters for the α−solvent, β−solvent, and α−β interactions are then fitted to the homopolymer + solvent and copolymer + solvent phase equilibria experimental data. Although this approach provides a more direct route to determining model parameters than copolymer-SAFT, the parameter regression becomes difficult when the corresponding homopolymer + solvent experimental data are not available.[19]

In general, a common limitation to the approaches used for determining SAFT model parameters for polymers is that the parameters are pulled together in a somewhat ad hoc way, which results in the need to fit pure-component and/or cross parameters to experimental polymer mixture data, thus reducing the predictive ability of the equation. To make the SAFT EOS a more predictive approach, parameters determined for small molecules need to be transferable to polymer systems in order to reduce the dependence on experimental data. Recently, several authors have combined group contribution approaches with the SAFT framework to better account for the effects of molecular structure and composition.[86−90,30] For example, Tobaly and co-workers[88−91] presented the GC-SAFT equation in which the functional group parameters are fitted to experimental vapor pressure and saturated liquid density data for different chemical families in successive steps according to the structure and composition of a molecule; however, for a given molecule, the group parameters are then averaged in order to describe molecules using a homonuclear-based approach. This strategy was later used by Tihic et al.[30,32] with the simplified PC-SAFT[92] equation of state to determine EOS parameters for several polymers. In this work, although an excellent description of the VLE for polymer systems such as polystyrene + toluene is obtained without adjusting any cross interactions, the majority of the systems studied include a binary interaction parameter fitted to experimental polymer mixture data. Additionally, we note that Lymperiadis et al.[86,93] have studied the liquid−liquid equilibria of the PE + pentane system with the SAFT-γ group contribution approach.[92]

In earlier work,[94] we developed a group-contribution-based SAFT-VR approach (GC-SAFT-VR) in order to develop a more physically realistic model for fluids, that is, one in which molecules are described by heterosegmented chains, i.e., chains of segments that can have different size and/or energy parameters. The retention of the groups within the chain term allows the connectivity of the groups within the molecule to be specified, thereby enabling the heterogeneity in molecular architecture to be captured within a SAFT model. Parameters were determined for several key functional groups (CH_3, CH_2, CH, CH_2=CH, C=O, C_6H_5, OCH_3 and OCH_2) by fitting to experimental vapor pressure and saturated liquid density data for a number of small molecules containing the functional groups of interest (i.e., alkanes, 1-alkenes, alkylbenzenes, ketones, esters). The transferability of the parameters obtained for each group was then tested by predicting the phase behavior of pure fluids not used in the fitting process and binary mixtures. In all cases, good agreement was obtained between the GC-SAFT-VR predictions and experimental data, and the ability of the GC-SAFT-VR equation to capture mixture phase behavior using only group parameters developed form pure fluids was demonstrated. In this work, we present parameters for additional key functional groups within the GC-SAFT-VR approach, including the OCH group in esters; the OCH_3, OCH_2, and OCH groups in ether molecules; the C−CH_2 group in branched alkanes; and the *cis*- and *trans*-CH=CH groups present in alkene molecules. These parameters are then used together in a transferable fashion to investigate the ability of the GC-SAFT-VR EOS to predict the phase behavior in polymer systems without fitting to any polymer data. In particular, we have studied the vapor−liquid equilibria of selected binary polymer solutions of LDPE (low-density polyethylene), PE (polyethylene), poly(1-heptene), poly(1-decene), *cis*-PBD (*cis*-1,4-polybutadiene), PS (polystyrene), PVME [poly(vinyl methyl ether)], PVAc [poly(vinyl acetate)], and PBMA [poly(*n*-butyl methacrylate)] with various solvents. Although the focus of this work is the prediction of VLE behavior, we have also considered liquid−liquid equilibria for the LDPE + *n*-hexane, polypropylene (PP) + diethyl ether, and PS + benzene systems to further test the versatility of the GC-SAFT-VR approach.

Model and Theory

In the GC-SAFT-VR approach, molecules are described as chains composed of tangentially bonded segments of different size and/or energy that represent each functional group present in the molecule. The segments interact via a square-well potential that is characterized by three parameters: the segment diameter σ, well depth ε, and potential range λ. In the case of polymer molecules, each polymer is described by segments that represent the functional groups comprising the polymer repeat unit, which are then connected together according to the polymer molecular composition and structure. In Figure 1, we provide the structures of the repeat units for the different polymer molecules studied. The simplest polymer considered is polyethylene (Figure 1a), in which the CH_2 group is the only functional group in the repeat unit. As the complexity in the structure of the polymer molecule varies, other functional groups are required to describe the functionality in the repeat unit. For example, in the case of PS (Figure 1e), which has a benzyl group attached to a hydrocarbon backbone, the GC-SAFT-VR model

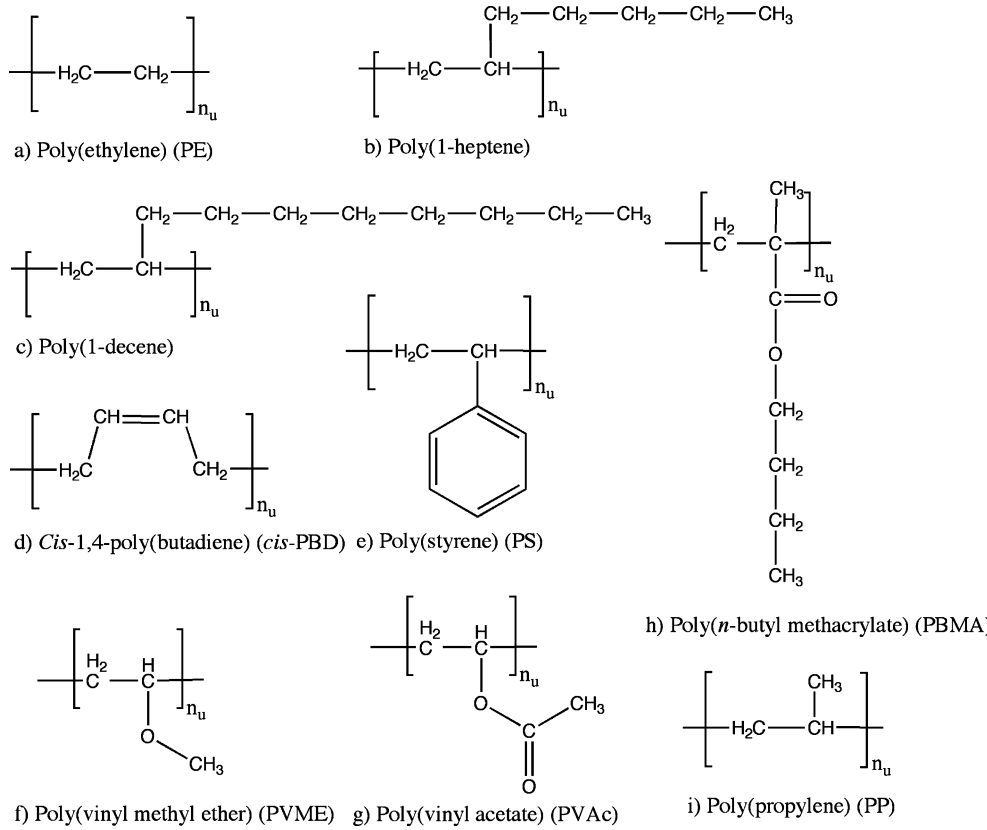

Figure 1. Repeat-unit structures for the polymer systems studied.

Table 1. GC-SAFT-VR Parameters for the Segment Size and Chain Length of Each Group Studied

group	σ (Å)	m_i
OCH (ester)	3.1616	0.5000
OCH_3 (ether)	3.1795	1.3300
OCH_2 (ether)	3.1235	1.0000
OCH (ether)	2.3691	0.9468
C—CH_2	3.3106	0.2866
cis-CH=CH	3.3489	0.8559
trans-CH=CH	3.4115	0.8559
C_6H_6	3.3522[a]	2.7521[a]

[a] Parameters taken from dos Ramos et al.[103]

for the polymer is represented by a CH_2 group attached to a CH group connected to the benzyl group (C_6H_5); hence, the polymer repeat unit for PS in our model is composed of three types of segments: CH, CH_2, and C_6H_5. Another example is the case of PVAc (Figure 1g), which has four functional groups in the repeat unit, namely, CH_3, CH_2, C=O, and OCH (ester) groups. As discussed in the Introduction, we previously obtained the optimized inter- and intramolecular parameters for the CH_3, CH_2, CH, C_6H_5, C=O, OCH_3 (ester), and OCH_2 (ester) functional groups (see Tables 1−3 of Peng et al.[87]), and the optimized parameters for the new functional groups [OCH (ester), OCH_3 (ether), OCH_2 (ether), OCH (ether), C—CH_2, *cis*-CH=CH, and *trans*-CH=CH] are presented in Tables 1−3 of this work. These parameters (number of segments m, segment diameter σ, segment−segment well depth ε, and potential range λ) were all obtained from the study of small molecules and are used in a transferable manner to describe the corresponding groups in the polymer repeat unit.

In the GC-SAFT-VR approach, the free energy of the fluid is written as the sum of four separate contributions

$$a = a^{\text{ideal}} + a^{\text{mono}} + a^{\text{chain}} + a^{\text{assoc}} \quad (1)$$

where a^{ideal} is the ideal free energy, a^{mono} is the contribution to the free energy due to the monomer segments, a^{chain} is the contribution due to the formation of bonds between monomer segments, and a^{assoc} is the contribution due to association interactions. The expressions for a^{assoc} are not included in this work because the systems studied are not associating fluids. The equations for each contribution to the free energy have been presented in previous work,[94] and so, here we only summarize the main expressions for each term with a particular focus on the application of the GC-SAFT-VR approach and model to polymer systems.

The ideal Helmholtz free energy is given by

$$a^{\text{ideal}} = \frac{A^{\text{ideal}}}{Nk_BT} = \sum_{k=1}^{n} x_k \ln \rho_k \Lambda_k^3 - 1 \quad (2)$$

where N represents the number of molecules; k_B is the Boltzmann constant; T is the temperature; n is the number of pure components; $\rho_k = N_k/V$ is the number density of chains of component k, where N_k is the number of molecules of component k and V is the total volume; x_k is the mole fraction of chains of component k in the mixture, and Λ_k is the thermal de Broglie wavelength.

As in the original SAFT-VR approach,[49,50] the monomer free energy is given by a second-order high-temperature expansion obtained using Barker and Henderson perturbation theory for mixtures,[95] viz.

$$a^{\text{mono}} = \frac{A^{\text{mono}}}{Nk_BT} = \sum_{k=1}^{n} \sum_{i=1}^{n'_k} x_k m_{ki} (a^{\text{HS}} + \beta a_1 + \beta^2 a_2) \quad (3)$$

where n'_k is the number of types of segment in component k; a^{HS} is the hard-sphere reference term; a_1 and a_2 are the first and second perturbation terms, respectively, associated with the attractive interactions; and m_{ki} is the overall chain-length of

Table 2. GC-SAFT-VR Segment−Segment Energy Well-Depth Parameters ε_{ij}/k_B (K)

type	OCH (ester)	OCH_3 (ether)	OCH_2 (ether)	OCH (ether)	$C-CH_2$	*cis*-CH=CH	*trans*-CH=CH	C_6H_6
CH_3	137.910	232.309	205.493	126.486	108.224	177.725	190.819	215.241
CH_2	138.784	233.782	206.796	127.288	108.911	178.852	192.029	216.606
CH	90.113[a]	151.796[a]	134.273[a]	82.648[a]	70.716[a]	116.129[a]	124.685[a]	140.643[a]
C=O	180.871	304.678[a]	269.508[a]	165.888[a]	141.938[a]	233.090[a]	250.262[a]	282.293
CH_2=CH	133.450[a]	224.797[a]	198.847[a]	122.395[a]	104.724[a]	171.978[a]	184.648[a]	208.280[a]
C_6H_5	97.447[a]	164.150	145.201	89.375[a]	76.471[a]	125.581[a]	134.832[a]	152.089
OCH_3 (ester)	112.532[a]	189.560[a]	167.679[a]	103.210[a]	88.309[a]	145.021[a]	155.705[a]	175.633
OCH_2 (ester)	92.844[a]	156.395[a]	138.342[a]	85.153[a]	72.859[a]	119.648[a]	128.463[a]	144.905
OCH (ester)	81.192	136.767[a]	120.980[a]	74.466[a]	63.715[a]	104.632[a]	112.341[a]	126.719[a]
OCH_3 (ether)	136.767[a]	230.385	203.791[a]	125.438[a]	107.328[a]	176.253[a]	189.238[a]	213.458
OCH_2 (ether)	120.980[a]	203.791[a]	180.266	110.958[a]	94.938[a]	155.907[a]	167.393[a]	188.818
OCH (ether)	74.466[a]	125.438[a]	110.958[a]	68.297	58.437[a]	95.965[a]	103.035[a]	116.222[a]
$C-CH_2$	63.715[a]	107.328[a]	94.938[a]	58.437[a]	50.000	82.110[a]	88.159[a]	99.442[a]
cis-CH=CH	104.632[a]	176.253[a]	155.907[a]	95.965[a]	82.110[a]	134.840	144.774[a]	163.303[a]
trans-CH=CH	112.341[a]	189.238[a]	167.393[a]	103.035[a]	88.159[a]	144.774[a]	155.440	175.334[a]
C_6H_6	126.719[a]	213.458	188.818	116.222[a]	99.442[a]	163.303[a]	175.334[a]	197.775[b]

[a] Assumes Lorentz−Berthelot combining rules. Cross interaction not yet tested. [b] Parameters taken from dos Ramos et al.[103]

Table 3. GC-SAFT-VR Segment−Segment Energy-Range Parameters λ_{ij}

type	OCH (ester)	OCH_3 (ether)	OCH_2 (ether)	OCH (ether)	$C-CH_2$	*cis*-CH=CH	*trans*-CH=CH	C_6H_6
CH_3	1.415	1.528	1.582	1.777	1.715	1.683	1.650	1.599
CH_2	1.517	1.568	1.677	1.874	1.802	1.771	1.738	1.691
CH	1.669[a]	1.778[a]	1.832[a]	2.051[a]	1.955[a]	1.923[a]	1.889[a]	1.842[a]
C=O	1.622	1.738[a]	1.796[a]	2.026[a]	1.928[a]	1.894[a]	1.857[a]	1.771
CH_2=CH	1.454[a]	1.569[a]	1.625[a]	1.830[a]	1.760[a]	1.727[a]	1.692[a]	1.641[a]
C_6H_5	1.673[a]	1.786	1.856	2.109[a]	1.993[a]	1.957[a]	1.918[a]	1.866
OCH_3 (ester)	1.488[a]	1.612[a]	1.672[a]	1.903[a]	1.816[a]	1.781[a]	1.743[a]	1.688
OCH_2 (ester)	1.464[a]	1.591[a]	1.653[a]	1.887[a]	1.800[a]	1.764[a]	1.726[a]	1.670
OCH (ester)	1.325	1.448[a]	1.506[a]	1.711[a]	1.653[a]	1.619[a]	1.583[a]	1.528[a]
OCH_3 (ether)	1.448[a]	1.570	1.629[a]	1.850[a]	1.772[a]	1.737[a]	1.701[a]	1.638
OCH_2 (ether)	1.506[a]	1.629[a]	1.690	1.921[a]	1.832[a]	1.797[a]	1.759[a]	1.705
OCH (ether)	1.711[a]	1.850[a]	1.921[a]	2.226	2.075[a]	2.033[a]	1.988[a]	1.929[a]
$C-CH_2$	1.653[a]	1.772[a]	1.832[a]	2.075[a]	1.966	1.931[a]	1.894[a]	1.842[a]
cis-CH=CH	1.619[a]	1.737[a]	1.797[a]	2.033[a]	1.931[a]	1.896	1.859[a]	1.808[a]
trans-CH=CH	1.583[a]	1.701[a]	1.759[a]	1.988[a]	1.894[a]	1.859[a]	1.823	1.772[a]
C_6H_6	1.528[a]	1.638	1.705	1.929[a]	1.842[a]	1.808[a]	1.772[a]	1.719[b]

[a] Assumes Lorentz−Berthelot combining rules. Cross interaction not yet tested. [b] Parameters taken from dos Ramos et al.[103]

the group of type i in component k. The residual free energy of the reference hard-sphere mixture is determined from the expression of Boublik[96] and Mansoori and co-workers[97] for multicomponent systems. The mean-attractive energy associated with the first-order perturbation term is treated in the context of the M1Xb mixing rule,[50] with the Padé expression proposed by Patel et al.[98] for the effective packing fraction used to calculate the hard-sphere radial distribution function. The second-order perturbation term is obtained using the local compressibility approximation.[49,50]

In the polymer−solvent systems studied, the overall chain length of segment type i in each solvent molecule is given by $m_{ki} = \nu_{si} m_i$, where ν_{si} is the number of segments of type i in the solvent and m_i is the chain length of one segment of type i. For the majority of the polymer systems studied, the polydispersity is not reported; therefore, for simplicity, we assumed that the polydispersity index of the polymers studied approaches unity, that is, the ratio between the weight-average molecular weight ($\bar{M}_w$) and the number-average molecular weight ($\bar{M}_n$) is equal to 1. In this case, the number of segments representing the functional groups in each polymer molecule is obtained from the number of repeat units within the polymer molecule (n_u), which can be calculated from the molecular weight of the polymer by dividing the total weight-average molecular weight of the polymer by the molecular weight of a single repeat unit ($\bar{M}_u$). Because the number of groups of each type within one repeat unit is also known (see Figure 1), the overall chain length of the functional group type i in the polymer can thus be obtained from $m_{ki} = \nu_{pi} m_i n_u$, that is, by multiplication of the number of repeat units (n_u), the chain length for a single group of type i (m_i), and the number of groups of type i within one repeat unit of the polymer (ν_{pi}). The values of n_u and ν_{pi} obtained for each polymer consider in this work are presented in Appendix A (Table A1). We note that, although we are excluding the polymer terminal groups when describing the structure of the polymer, we find very small differences between results obtained with and without the terminal groups, which is to be expected when considering such long chain molecules.

Finally, the chain term, a^{chain}, for a mixture of heterosegmented chain molecules is given by

$$a^{chain} = \frac{A^{chain}}{N k_B T} = -\sum_{k=1}^{n} x_k \sum_{ij} \ln y^{SW}_{ki,kj}(\sigma_{ki,kj}) \qquad (4)$$

where the first sum is over all components in the mixture and the second sum considers the chain formation and connectivity of the segments within a given chain. The background correlation function, $y^{SW}_{ki,kj}(\sigma_{ki,kj})$, is given by

$$y^{SW}_{ki,kj}(\sigma_{ki,kj}) = \exp(-\beta\varepsilon_{ki,kj})\, g^{SW}_{ki,kj}(\sigma_{ki,kj}) \qquad (5)$$

where $g^{SW}_{ki,kj}(\sigma_{ki,kj})$ is the radial distribution function for the square-well monomers and is approximated by a first-order high-temperature perturbation expansion.[49] The exact form of eq 4 naturally depends on the number of different types of functional groups and the connectivity of these groups in the molecules being studied. For example, if we consider the binary mixture of LDPE + n-pentane studied here, only two functional groups are used to model the mixture. The n-pentane molecule has two

terminal CH_3 groups, which we denote as segments of type 1 with parameters m_1, $\sigma_{11,11}$, $\varepsilon_{11,11}$, and $\lambda_{11,11}$; three CH_2 groups, which we denote as segments of type 2 with parameters m_2, $\sigma_{12,12}$, $\varepsilon_{12,12}$, and $\lambda_{12,12}$; two bonds between these functional groups (i.e., CH_2—CH_3); and two bonds between the CH_2 groups. The repeat unit of PE (as represented in Figure 1a) contains only two CH_2 groups, which are the same type as the CH_2 groups in *n*-pentane and are denoted by the parameters m_2, $\sigma_{22,22}$, $\varepsilon_{22,22}$, and $\lambda_{22,22}$, and there is only one bond between the CH_2 groups per repeat unit and in total $n_u - 1$ bonds connecting the repeat polymer units. In this case, eq 4 is given by

$$\frac{A^{\text{chain}}}{Nk_BT} = -x_1[2 \ln y^{SW}_{11,12}(\sigma_{11,12}) + 2 \ln y^{SW}_{12,12}(\sigma_{12,12}) + (2m_1 - 2) \ln y^{SW}_{11,11}(\sigma_{11,11}) + (3m_2 - 3) \ln y^{SW}_{12,12}(\sigma_{12,12})] - x_2[(2n_u m_2 - 1) \ln y^{SW}_{22,22}(\sigma_{22,22})] \quad (6)$$

where the first term in square brackets describes the *n*-pentane. Within this term are contributions due to the two bonds between segments of type 1 and type 2 [$2 \ln y^{SW}_{11,12}(\sigma_{11,12})$], the two bonds between segments of type 2 [$2 \ln y^{SW}_{12,12}(\sigma_{12,12})$], the chain formation contribution from the two CH_3 groups [$(2m_1 - 2) \ln y^{SW}_{11,11}(\sigma_{11,11})$], and the chain formation contribution from the three CH_2 groups [$(3m_2 - 3) \ln y^{SW}_{12,12}(\sigma_{12,12})$]. After simplification, this term reduces to

$$\frac{A^{\text{chain}}}{Nk_BT} = -x_1[2 \ln y^{SW}_{11,12}(\sigma_{11,12}) + (2m_1 - 2) \ln y^{SW}_{11,11}(\sigma_{11,11}) + (3m_2 - 1) \ln y^{SW}_{12,12}(\sigma_{12,12})] - x_2[(2n_u m_2 - 1) \ln y^{SW}_{22,22}(\sigma_{22,22})] \quad (7)$$

Similarly, the second term in square brackets corresponds to PE, and the terms shown after simplification through the collection of like terms correspond to the n_u bonds between segments of type 2 [$n_u \ln y^{SW}_{22,22}(\sigma_{22,22})$], $n_u - 1$ bonds between polymer repeat units [$(n_u - 1) \ln y^{SW}_{22,22}(\sigma_{22,22})$], and the contribution due to chain formation from the two CH_2 groups per repeat unit [$2n_u(m_2 - 1) \ln y^{SW}_{22,22}(\sigma_{22,22})$].

Once the Helmholtz free energy is determined, other thermodynamic properties, such as the chemical potential μ and compressibility factor Z, can be easily obtained using standard thermodynamic relations. In the vapor—liquid equilibrium (VLE) calculations, the polymer is assumed to be nonvolatile, and therefore, no polymer molecules are present in the gas phase; thus, the phase equilibria coexistence is obtained by equality of the total pressure and temperature in each phase and the equality of the chemical potential for the solvent in each phase.

Results

Parameterization of New Functional Groups in the GC-SAFT-VR Approach. To characterize the repeat units of a wide range of polymer systems, the molecular parameters for seven new functional groups that are present in the repeat units of *cis*-PBD, PVME, PVAc, and PBMA (Figure 1) must be determined. To summarize, we obtained parameters for the following groups: OCH to describe branched ester molecules, OCH_3, OCH_2, and OCH groups to describe ethers, *cis*-CH=CH and *trans*-CH=CH groups to describe the geometric isomers of the 1-alkene family, and the C—CH_2 group to enable the GC-SAFT-VR approach to describe branched molecules. The parameters were obtained by fitting to experimental data for vapor pressure and saturated liquid density for selected esters, ethers, *cis*-alkenes, *trans*-alkenes, and 2,2-dimethyl branched alkanes using an annealing technique.[99,100] Specifically, the molecular parameters for the OCH group in esters were determined by fitting to the experimental data for 2-propyl acetate and 2-butyl acetate, whereas parameters for the OCH group in ethers were fitted to the experimental data for 2-methoxypropane and 2-methoxybutane. The selection of candidates for the parameter fitting was guided by the available experimental data, which is somewhat limited for the branched alkyl ester and alkyl ether families. For the remaining functional groups, the compounds reported in Table 4 were selected for the fitting process. The parameters determined for each functional group are reported in Tables 1—3. Also included are the molecular parameters that describe the interactions between the new functional groups and those presented in our earlier work. In general, the parameters used for each functional group were chosen based on the deviations obtained from experimental vapor pressures and saturated liquid densities, while simultaneously ensuring that they were physically reasonable. For example, in Figure 2, we present the molecular parameters for the OCH_3, OCH_2, and OCH functional groups that describe the ester and ether families as a function of the molecular weight of the functional group. As can be seen from the figure, the set of parameters for the ester functional groups follows an almost linear trend as the molecular weight of the functional group is increased from OCH to OCH_2 and to OCH_3. A similar trend is observed for the parameters of the OCH_3 and OCH_2 functional groups in ethers; however, the parameters for chain length and potential range of the OCH ether group deviate somewhat from the linear behavior, which could be a consequence of the limited experimental data available for determining the parameters for this functional group. For functional groups with the same molecular weight, such as *cis*-CH=CH and *trans*-CH=CH, to check the suitability of the fitted parameters, we compared the values of $m\sigma^3$ and $m(\varepsilon/k_B)$ for the two functional groups. For the *trans*-CH=CH functional group, $m\sigma^3$ is equal to 33.9828, whereas for *cis*-CH=CH, the value of $m\sigma^3$ is 32.1462, which indicates that the *trans*-CH=CH functional group has a greater volume (i.e., is less dense) that the *cis*-CH=CH functional group. For the energy parameter, we obtained values of 133 and 115 for $m(\varepsilon/k_B)$ for the *trans*-CH=CH and *cis*-CH=CH functional groups respectively. The stronger energy parameter for the trans functional group can be interpreted as a stronger attractive interaction between the trans—trans functional group segments in the alkene molecules, which is consistent with the higher melting points observed for *trans*-alkenes compared to the corresponding *cis*-alkenes. For example, the melting points of the isomers of 2-butene are −106 and −139 °C for the trans and cis isomers, respectively.[101] Note that, although the potential range parameter (λ) also impacts the strength of the dispersion interaction, for the functional groups being considered, the values of λ are very similar.

As discussed in earlier work, within the GC-SAFT-VR approach cross-interaction parameters, which are needed between groups within a molecule as well as between groups in different molecules, can be determined from Lorentz—Berthelot combining rules or by fitting the cross-interaction to experimental data alongside the fitting of the new group parameters. Typically, the need for fitted cross interaction parameters can be anticipated based on expected deviations from Lorentz—Berthelot behavior when nonideal systems involving, for example, a highly polar component are being studied. In the development of new functional group parameters, the Lorentz—Berthelot combining rules are first tested, and if deviations between the GC-SAFT-VR predictions and experimental data

Table 4. Average Deviations in Vapor Pressures and Saturated Liquid Densities between Experimental Data[116] and Correlated Results for Some Pure Esters, Ethers, Branched Alkanes, *cis*-Alkenes, and *trans*-Alkenes

compound	T (K)	N_{pt}[a]	%AAD P[b]	%AAD ρ_{Liq}[c]
		OCH (ester)		
2-propyl acetate	210−500	30	10.86	2.14
2-butyl acetate	175−555	39	2.88	2.15
average			*6.87*	*2.15*
		OCH_3 (ether)		
dimethyl ether	140−390	26	3.28	2.44
1-methoxy ethane	170−430	27	7.89	1.22
1-methoxy propane	140−470	34	9.21	2.00
1-methoxy butane	160−510	36	4.73	1.60
1-methoxy pentane	180−540	37	5.89	1.28
average			*6.20*	*1.71*
		OCH_2 (ether)		
dipropyl ether	155−525	38	8.82	1.91
dibutyl ether	180−580	41	11.02	2.12
1-ethoxy propane	160−490	33	13.49	1.93
1-ethoxy butane	180−520	35	2.39	1.67
1-ethoxy hexane	190−570	39	8.05	1.43
average			*8.75*	*1.81*
		OCH (ether)		
2-methoxypropane	150−415	54	3.73	1.07
2-methoxybutane	150−445	60	6.62	2.03
average			*5.18*	*1.55*
		C−CH_2		
2,2-dimethyl butane	180−440	27	5.42	0.98
2,2-dimethyl pentane	150−470	33	7.50	1.29
2,2-dimethyl hexane	160−500	35	5.95	1.30
2,2-dimethyl heptane	170−520	36	4.90	1.07
2,2-dimethyl octane	235−555	33	4.41	1.57
average			*5.64*	*1.24*
		cis-CH═CH		
cis-2-pentene	125−475	36	12.54	4.69
cis-3-hexene	140−509	36	3.65	3.40
cis-2-heptene	165−545	39	4.09	2.85
cis-3-heptene	140−545	42	3.06	4.09
cis-2-octene	175−570	41	4.13	3.52
cis-4-octene	155−565	42	8.33	2.64
cis-2-decene	210−620	42	2.84	7.44
average			*5.52*	*4.09*
		trans-CH═CH		
trans-2-butene	170−428	27	2.70	4.88
trans-2-pentene	135−470	35	6.97	2.79
trans-3-hexene	160−509	36	3.29	4.04
trans-2-heptene	165−540	39	2.89	2.99
trans-3-heptene	140−540	41	3.73	3.71
trans-2-octene	190−575	40	8.63	3.01
trans-3-octene	165−570	42	7.77	2.59
trans-4-octene	180−570	40	8.73	2.46
trans-2-decene	220−615	41	2.74	7.19
average			*5.27*	*3.74*
overall average			**6.20**	**2.33**

[a] N_{pt} corresponds to the number of data points used in the optimizaton process.

[b]
$$\%\text{AAD } P = \frac{1}{N_{pt}} \sum_{i=1}^{N_{pt}} \left| \frac{P_i^{theo} - P_i^{exp}}{P_i^{exp}} \right| \times 100\%$$

[c]
$$\%\text{AAD } \rho_{Liq} = \frac{1}{N_{pt}} \sum_{i=1}^{N_{pt}} \left| \frac{\rho_{Liq_i}^{theo} - \rho_{Liq_i}^{exp}}{\rho_{Liq_i}^{exp}} \right| \times 100\%$$

for the pure fluid are observed, new group parameters and cross interactions are fitted simultaneously. In this work, it was found that non-Lorentz−Berthelot cross-interaction parameters were needed for the OCH_3 (ether)−benzene, C═O−benzene, and OCH_3 (ether)−CH_2 interactions. Therefore, the parameters for the OCH_3 (ether)−CH_2 interaction was fitted alongside the OCH_3 (ether) parameters from a fit to pure ether experimental data. The benzene systems are discussed separately below. For all of the new molecules studied, the percentages for the absolute average deviation of the calculated vapor pressures (%AAD P) and liquid densities (%AAD ρ_{Liq}) from the experimental values are presented in Table 4. For the saturated liquid density, we obtained an overall deviation of 2.33%, and for the vapor pressures, a slightly higher value of 6.20%, which could be due to the fact that a wider temperature range was used in the fitting process, including data at temperatures near the triple point, which has been shown to affect the deviations as discussed by Laffite et al.[102]

Although benzene could be considered the "zeroth" member of the alkylbenzene family, it is quite different from the other family members because no alkyl chain is connected to the benzenyl ring; for this reason, we decided to describe the benzene molecule as a single functional group (C_6H_6). Although one could decompose the benzene and benzyl rings into CH groups, we noted that this approach, when used in the work of Lymperiadis et al. with the SAFT-γ equation,[86] did not appear to significantly improve agreement with the experimental data. The intermolecular parameters (m, σ, ε, and λ) for benzene included in Tables 1−3 were therefore taken from the work of dos Ramos et al.[103] Given the quadrupole nature of the benzene ring, we would expect the cross interactions between the benzene ring and other functional groups, such as the carbonyl and ether groups, to deviate from the ideal behavior predicted by the Lorentz−Berthelot combining rules. Furthermore, because these cross interactions are not encountered in the small molecules that were used to fit the model parameters for these functional groups, we cannot fit the cross interactions to pure-fluid experimental data. Therefore, to correctly account for such cross interactions, we can either determine the cross-group parameters by studying small-molecule mixtures containing the appropriate groups or use mixture polymer data. We adopted the former approach because the main aim of this work was to develop a fully predictive method for studying polymer systems. Specifically, we fitted the cross interaction between the OCH group and the benzene group and between the C═O group and the benzene group to experimental data for the benzene + 1-methoxybutane and benzene + butyl acetate binary mixtures, respectively. In developing these parameters, we considered a number of factors, as summarized by the results shown in Figure 3: In Figure 3a, we present the vapor−liquid equilibrium of benzene + butylbenzene at 353.15 and 363.15 K. Here, the theoretical predictions used the Lorentz−Berthelot combining rules for unlike interactions between functional groups. From the figure, it can be seen that the theory is able to correctly predict the phase behavior, indicating that the unlike benzene−benzenyl ring interactions are described. From these results, we anticipate that the interactions of the benzene ring with other functional groups will behave similarly to the benzenyl group with other functional groups, and vice versa. In part b of Figure 3, the phase behavior of the ethylbenzene + dipropyl ether binary mixture at different temperatures are considered to test the OCH_2 (ether)−benzenyl group interaction. Here, we see that the theory is able to predict the phase behavior; however, a small deviation is seen as the composition approaches pure dipropylether because of an underprediction of the vapor pressure of this component (see deviations reported in Table 4). The binary mixture of benzene + butyl acetate is studied in Figure 3c. As anticipated, and can be seen from the figure, the theoretical predictions for the VLE deviate from the experimental data when

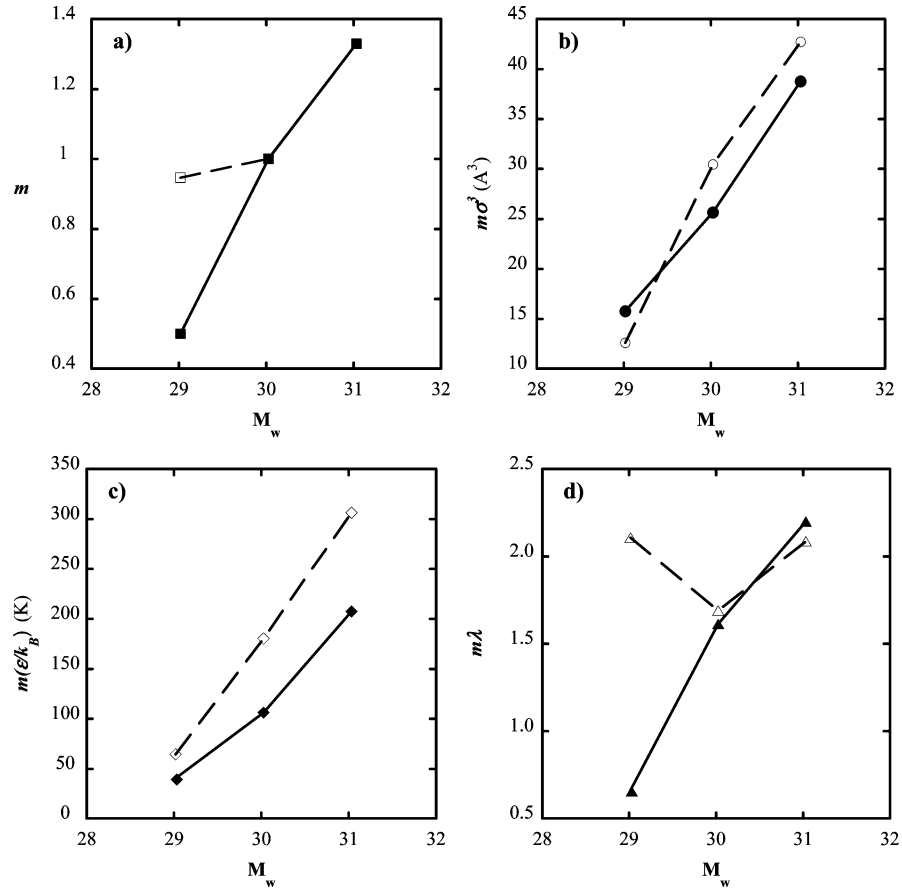

Figure 2. GC-SAFT-VR parameters for the functional groups OCH_3, OCH_2, and OCH for ester (solid symbols) and ether (open symbols) molecules as a function of the molecular weight: (a) chain length, (b) segment size, (c) potential depth, and (d) potential range. (Lines are provided as a guide to the eye only.)

a polar functional group is present. The cross-interaction parameters between the carbonyl group (C═O) and benzene ring (C_6H_6) in the binary mixture were therefore modified by fitting the segment−segment energy range parameter (λ_{ij}) between the carbonyl group (C═O) in butyl acetate and the benzene ring (C_6H_6) to the VLE curve for the benzene + butyl acetate system at 1.01325 bar, giving a value for λ_{ij} (C═O−C_6H_6) of 1.771. From this value, using a combining rule for the cross range parameter, viz.

$$\lambda_{ij} = \gamma_{ij}\left(\frac{\lambda_{ii}\sigma_{ii} + \lambda_{jj}\sigma_{jj}}{\sigma_{ii} + \sigma_{jj}}\right)$$

one obtains $\gamma_{ij} = 0.98$. γ_{ij} is then used in a transferable manner to determine the cross carbonyl−benzenyl group interaction [λ_{ij}(C═O−C_6H_5) = 1.914]. Note that this value (λ_{ij} = 1.914) is different from the one presented in our previous work[87] (see Table 3, λ_{ij} = 1.953), because, as noted in ref 87, we assumed Lorentz−Berthelot combining rules for cross interactions not yet studied. Finally, we considered the mixture of benzene + 1-methoxybutane to test the cross interactions between the benzene group and the OCH_3 ether group, as shown in Figure 3d. Again, the theory deviates from the VLE experimental data for this system, and so, the segment−segment energy range cross-interaction parameter between the carbonyl group (C═O) and the benzene ring was fitted to the VLE curve for the benzene + 1-methoxybutane system at 343.15 K, giving a value for λ_{ij} [OCH_3 (ether)−C_6H_6] of 1.638 (or γ_{ij} = 0.995); the value of γ_{ij} = 0.995 was then used in a transferable manner to modify the cross OCH_3 (ether)−benzenyl group interaction.

Polymeric Systems. We first consider mixtures of LDPE with linear alkanes and alkenes. In Figure 4a, we present the theoretical predictions for the solubility of *n*-pentane ($CH_3CH_2CH_2CH_2CH_3$) and 1-pentene (CH_2═$CHCH_2CH_2CH_3$) in LDPE with a weight-average molecular weight ($\bar{M}_w$) of 76 000 g/mol at temperatures of 423.65 and 474.15 K. Good agreement between the experimental data and theoretical predictions was obtained for both systems at 423.65 K, although we note a slight overprediction of the pressure at the higher temperature (474.15 K), which is above the critical temperatures of both *n*-pentane (469 K)[104] and 1-pentene (465 K).[104] This is to be expected since the GC-SAFT-VR equation is an analytical EOS and does not consider the crossover to nonanalytical behavior due to the density fluctuations that occur in real fluids in the critical region, resulting in overprediction of the critical point.[54,55,60,61] From Figure 4a, we also note how the theory is able to predict the experimentally observed differences in phase behavior between *n*-pentane and 1-pentene, that is, more *n*-pentane than 1-pentene is absorbed in the LDPE at the same pressure and temperature. Overall, the agreement between the theoretical predictions and experimental data is very good given that no polymer data were used to obtain the model parameters and no additional binary interaction parameters between the polymer and solvent were used. In Figure 4a, we also include results for the PE + *n*-pentane system obtained from the original SAFT-VR approach, where the PE and *n*-pentane homonuclear chain parameters were determined from the work of Paricaud et al.[105] and are based on those for the *n*-alkanes. As can be seen from the figure, both approaches can successfully describe the absorption of pentane in PE: At the lower temperature evaluated, the original SAFT-VR curve is in better agreement with the experimental data, whereas at the higher temperature, the GC-SAFT-VR approach provides the better prediction. In

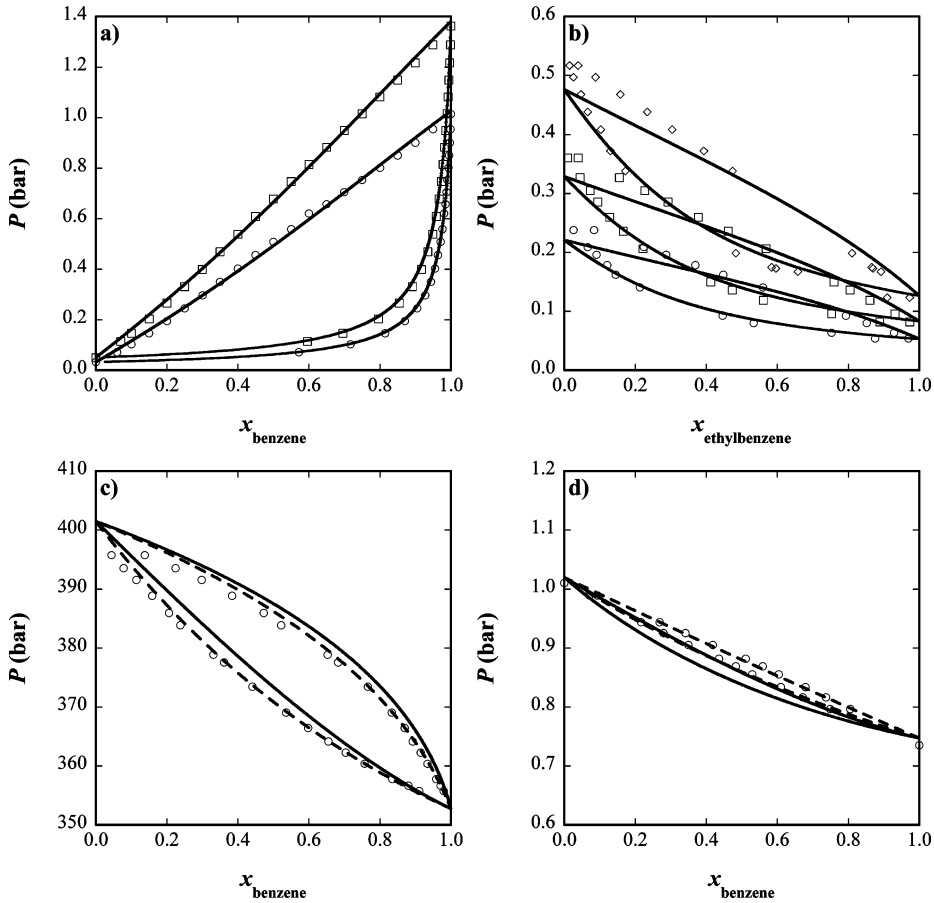

Figure 3. Vapor−liquid equilibria for binary mixtures of (a) benzene + butylbenzene, (b) ethylbenzene + dipropylether, (c) benzene + butyl acetate, and (d) benzene + 1-methoxybutane. The solid lines correspond to the theoretical predictions from the GC-SAFT-VR approach using Lorentz−Berthelot combining rules, and the dashed lines represent the calculations obtained when modified cross parameters are used (see text). Experimental data[117−120] are represented by the symbols: benzene + butylbenzene at (○) 353.15 and (□) 363.15 K; ethylbenzene + dipropylether at (○) 323.15, (□) 333.15, and (◇) 343.15 K; benzene + butyl acetate at 1.01325 bar (○); and benzene + 1-methoxybutane at 343.15 K (○).

Figure 4b, we provide an additional comparison between the GC-SAFT-VR and original SAFT-VR approaches for the solubility of 1-butene in LDPE from the work of Haslam and co-workers.[108] In this study, the authors compared the ability of the original SAFT-VR and PC-SAFT approaches to describe the phase behavior of several PE-based systems and found that the two approaches generally performed equally well, with the SAFT-VR equation requiring the use of a binary interaction parameter fitted to polymer mixture data for almost all of the systems studied and the PC-SAFT equation requiring one for two of the five systems studied. In general, the predictions from the GC-SAFT-VR and original SAFT-VR equations are comparable, as seen in Figure 4a,b; however, it is clear that the main advantage of the GC-SAFT-VR approach in studying polymer systems lies in the ability to describe complex polymers, such as PS, PP, PVAc, PMVE, without the need to fit either the pure-polymer parameters or cross interactions to experimental polymer data. With the SAFT-VR approach, there is no means by which to determine these parameters other than to fit to polymer *PVT* and binary VLE data. Additionally, given that, even for systems involving simple polymers (i.e., PE, which has no functional groups beyond CH_2 and no polarity), binary interaction parameters are needed with the original SAFT-VR approach to obtain good agreement with experimental data, they will be needed in the study of more complex polymer systems. Whereas, for the SAFT-VR equation, these parameters must be fitted to binary polymer VLE data, thus reducing the predictive capability of the approach further still, cross interactions in the GC-SAFT-VR approach are determined from small-molecule data, with no polymer data being used.

We next studied the PE + toluene system in order to examine the effect of the number-average molecular weight ($\bar{M}_n$) of the polymer on the VLE as a function of the weight fraction of the solvent in the liquid phase (w_1). As can be seen in Figure 5, the theoretical predictions are in good agreement with the experimental data, again considering that no polymer data were used to describe the phase behavior of this system. For the PE system with a higher molecular weight ($\bar{M}_n = 6220$ g/mol), the theory predicts a lower weight fraction of toluene absorbed than for the system with a lower molecular weight ($\bar{M}_n = 1710$ g/mol) at the same temperature and pressure, in agreement with the experimental data. We note that the effect of the number-average molecular weight of the PE on the phase behavior is small.

We next considered the phase behavior of two different branched polyolefins in toluene. Figure 6a presents the experimental weight fractions of toluene in poly(1-decene) and poly(1-heptene) at 303.15 K, compared with predictions obtained from the GC-SAFT-VR EOS. Although poly(1-decene) ($\bar{M}_n$ = 213 900 g/mol) and poly(1-heptene) ($\bar{M}_n = 224\,100$ g/mol) have similar molecular weights, they differ in structure, as illustrated in Figure 1b,c (and in Table A1, Appendix A); specifically, the poly(1-decene) repeat unit has three additional CH_2 functional groups than the poly(1-heptene) repeat unit. The predicted curve for the poly(1-decene) system with long branches is slightly below that for poly(1-heptene) with short branches, which is in agreement with the experimental data; however, the effect of

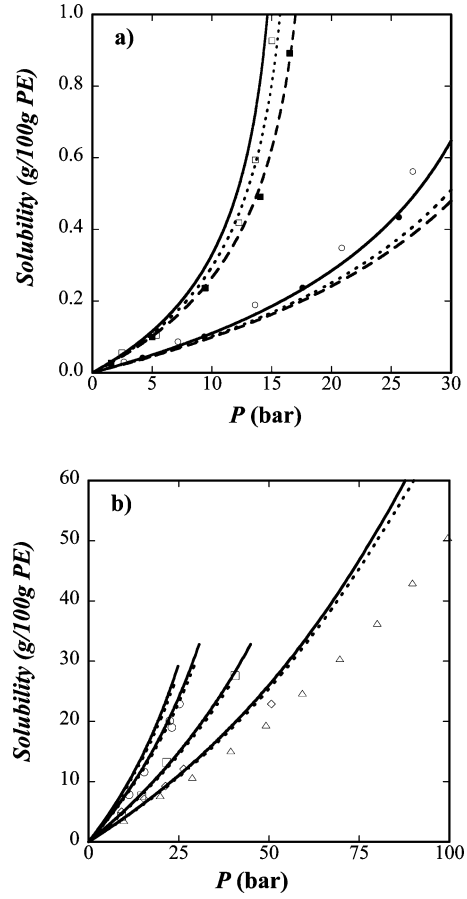

Figure 4. Solubilities of alkanes and alkenes in LDPE. (a) *n*-Pentane in LDPE ($\bar{M}_w$ = 76 000 g/mol) and 1-pentene in LDPE ($\bar{M}_w$ = 76 000 g/mol) at 423.65 and 474.15 K. The solid and dashed lines correspond to the GC-SAFT-VR predictions for the *n*-pentane and 1-pentene systems, respectively, and the dotted lines correspond to predictions from the original SAFT-VR equation for the PE + *n*-pentane system. Experimental data[121] for *n*-pentane + LDPE at (□) 423.65 and (○) 474.15 K and for 1-pentene + LDPE at (■) 423.65 and (●) 474.15 K are also included. (b) 1-Butene in LDPE ($\bar{M}_n$ = 1940 g/mol) at 428.15, 438.15, 468.15, and 493.15 K. The solid lines correspond to the GC-SAFT-VR predictions for the 1-butene system, and the dotted lines correspond to predictions from the original SAFT-VR equation. Experimental data[106,107] for 1-butene + LDPE at (□) 428.15, (○) 438.15, (◇) 468.15, and (Δ) 493.15 K are also included.

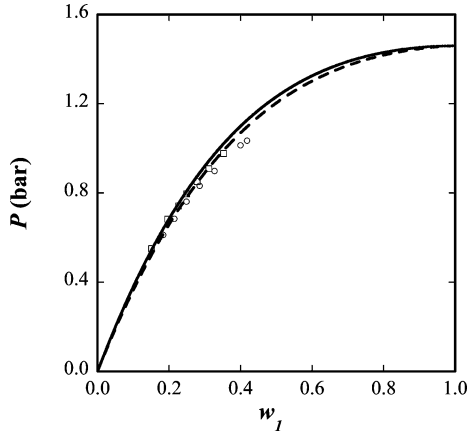

Figure 5. Constant-temperature $P-w$ slices of the phase diagram for toluene (1) + PE (2) at 393.15 K and different polymer molecular weights. The solid and dashed lines correspond to the GC-SAFT-VR predictions at $\bar{M}_n$ = 6220 and 1710 g/mol, respectively. The experimental data[122] are represented by the symbols for $\bar{M}_n$ = (□) 6220 and (○) 1710 g/mol.

branching on the VLE of these high-molecular-weight polyolefins was found to be largely insignificant for both the theoretical predictions and experimental data. As can be seen

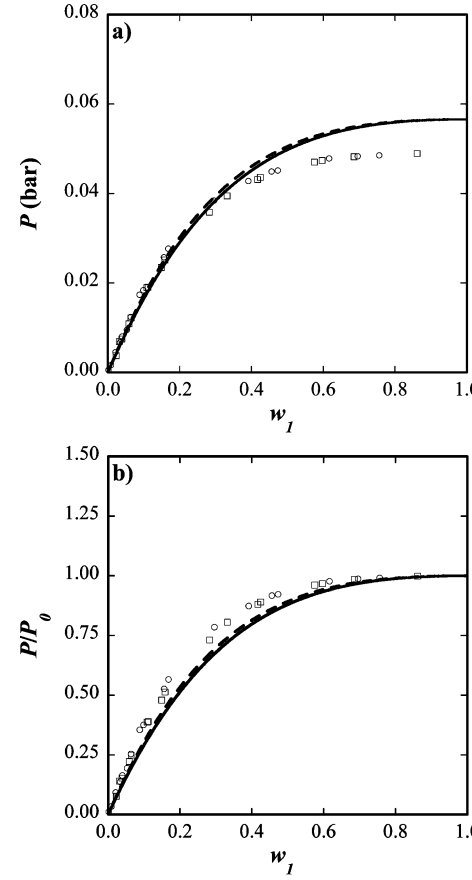

Figure 6. Constant-temperature $P-w$ slices of the phase diagram of toluene (1) + poly(1-decene) (2) ($\bar{M}_n$ = 213 900 g/mol) and toluene (1) + poly(1-heptene) (2) ($\bar{M}_n$ = 224 100 g/mol) at 303.15 K. The solid lines correspond to GC-SAFT-VR predictions for the poly(1-decene) system, and the dashed lines correspond to the poly(1-heptene) system. Experimental data[122] at 303.15 K are represented by the symbols for poly(1-decene) (□) and poly(1-heptene) (○). In a, the vapor pressure is given in real units (bar), and in b, the vapor pressure is reduced by the pure-solvent saturation pressure (P_0).

from Figure 6a, the theoretical predictions are in good overall agreement with the experimental data, although the absorption of toluene in poly(1-decene) or poly(1-heptene) is under predicted when the weight fraction of toluene is above 0.4. At higher weight fractions, the experimental data exhibit a flat behavior, indicating that there is no change in pressure with composition and, therefore, the pressure of the system will be determined predominately by the vapor pressure of pure toluene. Then, the deviation between the theoretical predictions and experimental data is therefore due to the overprediction of the vapor pressure of pure toluene. This is further underscored if one considers Figure 6b in which very good agreement with experimental data is obtained when the pressure is reduced with respect to the pure solvent saturation pressure. During the parameter regression for the pure alkylbenzene family, we noted that although the %AAD values obtained for the vapor pressure and saturated liquid density were good (4.70% and 3.76% respectively),[94] the shape of the predicted liquid density is less curved than that observed experimentally. This could be due to the description of the C_6H_5 group as a single entity; however, as noted earlier, similar deviations from experimental data are seen in the SAFT-γ approach, which models each carbon and its associated hydrogens in the benzene ring by separate segments.[86] An alternative explanation could be that the quadrupolar interactions of the benzene molecule are not explicitly included in the model.[109]

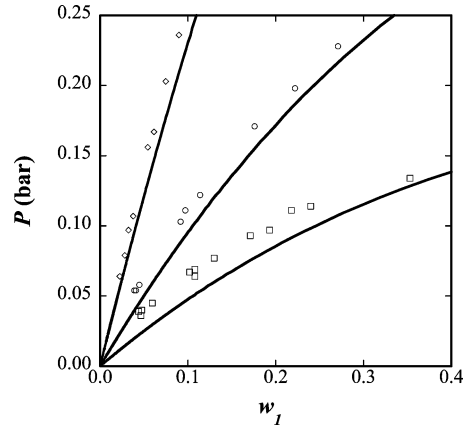

Figure 7. GC-SAFT-VR predictions of constant-temperature $P-w$ slices of the phase diagram for ethylbenzene (1) + *cis*-1,4 PBD (2) ($\bar{M}_w$ = 250 000 g/mol) and (□) 353.15, (○) 373.15, and (◇) 403.15 K compared to experimental data.[123] The lines correspond to the theoretical predictions.

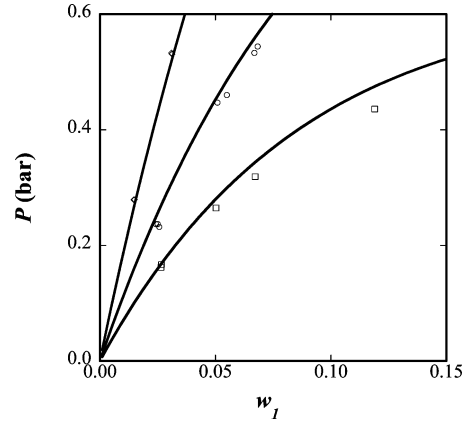

Figure 8. GC-SAFT-VR predictions of constant-temperature $P-w$ slices of the phase diagram for nonane (1) + PS (2) ($\bar{M}_n$ = 53 700 g/mol) at T = (□) 403.15, (○) 423.15, and (◇) 448.15 K compared to experimental data.[123] The lines correspond to the theoretical predictions.

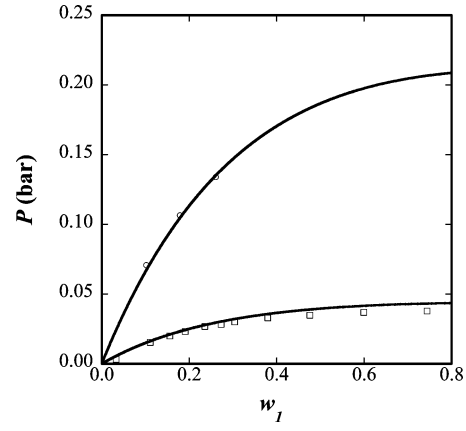

Figure 9. GC-SAFT-VR predictions of constant-temperature $P-w$ slices of the phase diagram for toluene (1) + PS (2) ($\bar{M}_n$ = 290 000 g/mol) at T = (□) 298.15 and (○) 333.15 K compared to experimental data.[123] The lines correspond to the theoretical predictions.

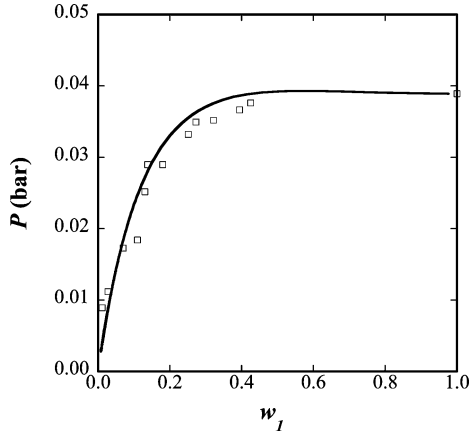

Figure 10. GC-SAFT-VR predictions of a constant-temperature $P-w$ slice of the phase diagram for 3-pentanone (1) + PS (2) ($\bar{M}_n$ = 200 000 g/mol) at 293.15 K (□) compared to experimental data.[123] The solid line corresponds to the theoretical predictions.

In contrast to the linear polyolefins studied so far, *cis*-1,4-poly(butadiene) (*cis*-PBD) has a backbone structure that is composed of two different segments: *cis*-CH═CH and CH_2 (see Figure 1d). The predicted VLE behavior of *cis*-PBD ($\bar{M}_w$ = 250 000 g/mol) and ethylbenzene at 353.15, 373.15, and 403.15 K compared to experimental data is presented in Figure 7. As the temperature increases, experimentally, less ethyl benzene is absorbed in the *cis*-PBD at the same pressure, which is accurately captured by the theory. Despite the complexity in the structure of the system, namely, the presence of the benzenyl ring in the solvent and the covalent double bond in the polymer, the results from the theory are in good agreement with the experimental data, although we note a slight overprediction of the solubility, particularly at the lower temperature. As discussed previously, we speculate that this is due to the inadequate representation of the interactions between the polymer and the benzene ring in the solvent.

Having studied the VLE behavior of some linear and branched polyolefin solutions, we next turned to polymers containing other chemical groups. We first examined the VLE phase behavior of mixtures of PS, which has a benzyl functional group pendant to the polymer backbone as illustrated in Figure 1e. The results obtained from the GC-SAFT-VR EOS for the *n*-nonane + PS binary mixture for a polymer sample with $\bar{M}_n$ = 53 700 g/mol at 403.15, 423.15, and 448.15 K are presented in Figure 8. From this figure, we can see that the model predicts the VLE behavior of this system accurately as a function of temperature, again without the use of polymer experimental data or binary parameters fitted to the *n*-nonane + PS system. Similarly, for the toluene + PS system ($\bar{M}_n$ = 290 000 g/mol), as shown in Figure 9 at 298.15 and 333.15 K, we find that the theoretical predictions for the VLE are also in good agreement with experimental data, indicating that the theory is able to describe the thermodynamic behavior of PS in different types of solvents.

We next applied the GC-SAFTVR EOS to investigate the VLE behavior of PS in polar solvents such as ketones and esters. The results from VLE calculations for the 3-pentanone + PS system ($\bar{M}_n$ = 200 000 g/mol) at 293.15 K are presented in Figure 10. As can be seen from the figure, the predictions from the GC-SAFT-VR theory using the group parameters (CH_3, CH_2, and C═O for 3-pentanone and CH_2, CH, and benzyl ring for PS) fitted to small molecules are in good agreement with the experimental data. We also studied the PS ($\bar{M}_n$ = 290 000 g/mol) + 2-butanone system at 298.15 and 343.15 K, the results of which are presented in Figure 11, along with the corresponding experimental data. As can be seen from the figure, the theory accurately predicts the VLE of the 2-butanone + PS system with only a small deviation from the experimental data, seen as the weight composition approaches the pure-solvent fraction. Although the systems shown in Figures 10 and 11 are not at exactly the same thermodynamic conditions and the same molecular weight, a comparison between the figures illustrates the ability of the GC-SAFT-VR approach to capture the changes in phase behavior between the 2-butanone and 3-pentanone systems by simply adding a CH_2 group to the solvent molecule

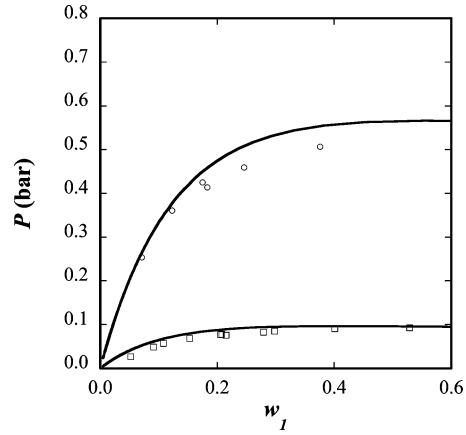

Figure 11. GC-SAFT-VR predictions of constant-temperature $P-w$ slices of the phase diagram for 2-butanone (1) + PS (2) ($\bar{M}_w$ = 290 000 g/mol) at (□) 298.15 and (○) 343.15 K compared to experimental data.[123] The solid lines correspond to theoretical predictions.

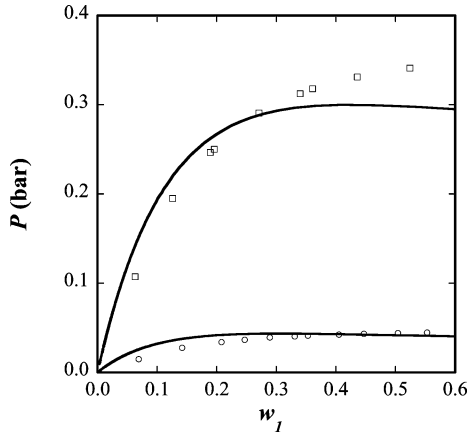

Figure 12. GC-SAFT-VR predictions of constant-temperature $P-w$ slices of the phase diagram for propyl acetate (1) + PS (2) ($\bar{M}_n$ = 290 000 g/mol) at (○) 298.15 and (□) 343.15 K compared to experimental data.[123] The solid lines correspond to the theoretical predictions.

and specifying the new location of the carbonyl group. We also examined the phase equilibria of the system containing PS ($\bar{M}_n$ = 290 000 g/mol) and *n*-propyl acetate ($CH_3C{=}OOCH_2CH_2CH_3$) at 298.15 and 343.15 K. We again see from Figure 12 that the GC-SAFT-VR approach is able to accurately predict the VLE behavior. Comparing Figures 11 and 12 at the same temperature, we note that the theory accurately captures the effect of changing the polymer structure from 2-butanone to propyl acetate (i.e., by adding the ester group OCH_2), by shifting the curve toward lower pressures.

Increasing the complexity of the polymer further still, we next considered polymer systems containing PVME, whose repeat unit contains CH_2, CH, and CH_3O (ether) functional groups (see Figure 1f), and PVAc, whose repeat unit also contains the polar carbonyl group (see Figure 1g). Figure 13 presents the VLE behavior for the systems PVME + benzene and PVME + toluene at 323.15 and 343.15 K and the system PVME + ethyl benzene at 373.15 and 398.15 K. From the figure, we note that the theoretical predictions are again in good agreement with the experimental VLE data, with the theory correctly describing the shift of the VLE curve to higher pressures as the temperature increases. Additionally, the effect of changing the solvent used in the PVME mixtures can be assessed by comparing the results obtained at similar thermodynamic conditions; the curve for benzene + PVME at 323.15 K is located at higher pressures than that observed for toluene + PVME at 323.15 K, indicating that more toluene than benzene is absorbed in PVME at the same pressure and temperature, which is accurately

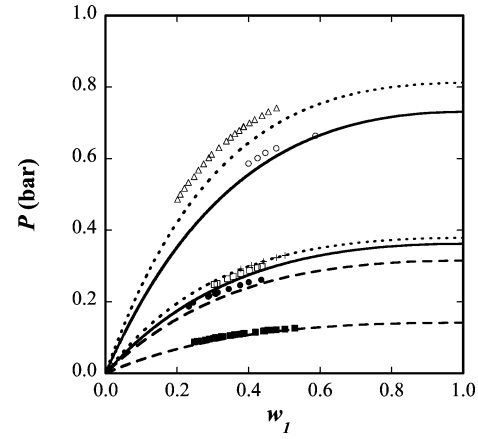

Figure 13. Constant-temperature $P-w$ slices of the phase diagram for benzene (1) + PVME (2), toluene (1) + PVME (2), and ethylbenzene (1) + PVME (2) ($\bar{M}_n$ = 14 600 g/mol). The solid, dashed, and dotted lines correspond to the GC-SAFT-VR predictions for the benzene, toluene, and ethylbenzene systems, respectively. The experimental data[122] correspond to the following symbols: benzene + PVME at (□) 323.15 and (○) 343.15 K; toluene + PVME at (■) 323.15 and (●) 343.15 K; and ethylbenzene + PVME at (×) 373.15 and (Δ) 398.15 K.

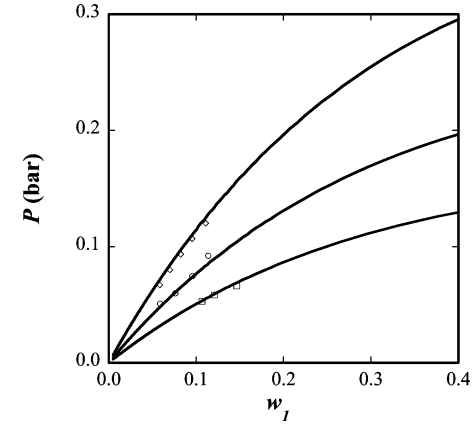

Figure 14. GC-SAFT-VR predictions of constant-temperature $P-w$ slices of the phase diagram for benzene (1) + PVAc (2) ($\bar{M}_n$ = 170 000 g/mol) at (□) 303.15, (○) 313.15, and (◇) 323.15 K compared to experimental data.[123] The solid lines correspond to the theoretical predictions.

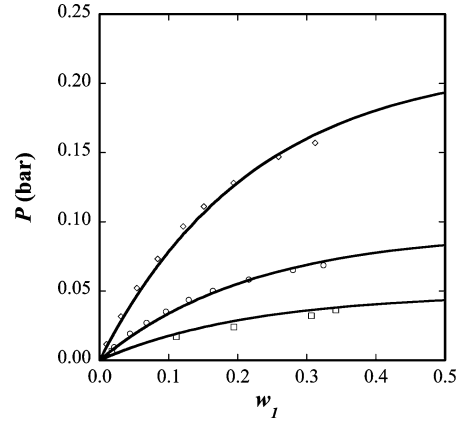

Figure 15. GC-SAFT-VR predictions of constant-temperature $P-w$ slices of the phase diagram for toluene (1) + PVAc (2) at (□) 299.55 ($\bar{M}_n$ = 320 000 g/mol), (○) 313.15 ($\bar{M}_n$ = 158000 g/mol), and (◇) 333.15 K ($\bar{M}_n$ = 158000 g/mol) compared to experimental data.[122] The solid lines correspond to the theoretical predictions.

captured by the theoretical predictions. In Figures 14−16, we present GC-SAFT-VR predictions for the VLE of the PVAc + benzene, toluene, and acetone systems, respectively, at different temperatures. For PVAc + benzene (Figure 14), we see that the

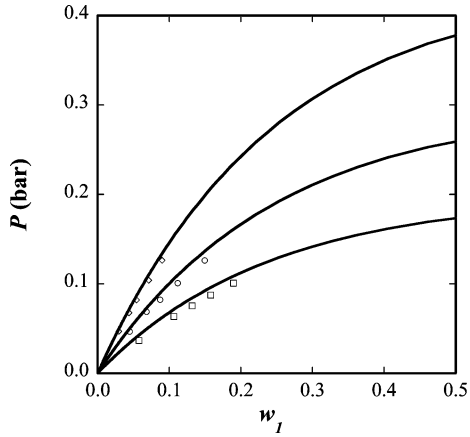

Figure 16. GC-SAFT-VR predictions of constant-temperature $P-w$ slices of the phase diagram for acetone (1) + PVAc (2) ($\bar{M}_n$ = 170 000 g/mol) at (□) 303.15, (○) 313.15, and (◇) 323.15 K compared to experimental data.[122] The solid lines correspond to theoretical predictions.

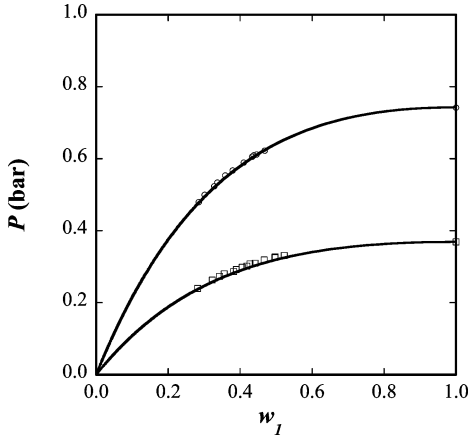

Figure 17. GC-SAFT-VR predictions of constant-temperature $P-w$ slices of the phase diagram for benzene (1) + PBMA (2) ($\bar{M}_n$ = 36 800 g/mol) at (□) 323.65 and (○) 343.65 K compared to experimental data.[122] The solid lines correspond to theoretical predictions.

theoretical predictions are in an excellent agreement with the experimental data, considering that no polymer data were used to determine the GC-SAFT-VR parameters. For both the PVAc + toluene and PVAc + acetone systems (Figures 15 and 16, respectively), excellent agreement between the theoretical predictions and experimental data is again observed, which further demonstrates the transferability of the parameters previously obtained.

Finally, we investigated the VLE of PBMA in benzene and ethylbenzene at different temperatures. One of the advantages of the GC-SAFT-VR approach is that the different functional groups within the polymer repeat unit can be specified explicitly at both the monomer and chain levels of the theory, thus allowing group connectivity to be described and complex polymers such as PBMA to be explicitly modeled. In Figure 17, we present the absorption curves for the system of benzene + PMBA at 323.65 and 343.65 K, which can be seen to exhibit excellent agreement with the experimental data. Similarly, the phase diagram of ethylbenzene + PMBA at 343.65, 373.15, and 403.15 K in Figure 18 shows good agreement with the experimental data; however, a small deviation is observed when the curve at 403.15 K approaches the pure-solvent region. The deviation mainly comes from the slight overprediction of the pure vapor pressure for ethylbenzene, which, as discussed in Peng et al.,[87] could be caused by the description of C_6H_5 as a single group.

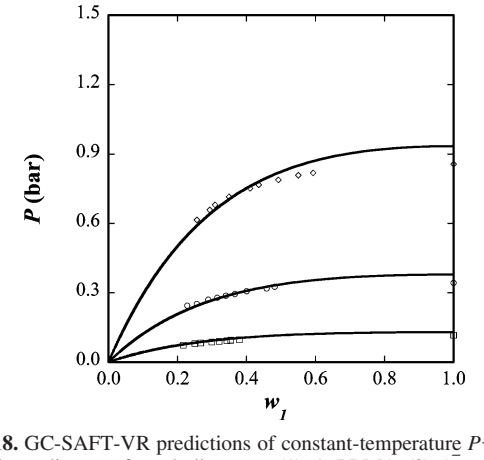

Figure 18. GC-SAFT-VR predictions of constant-temperature $P-w$ slices of the phase diagram for ethylbenzene (1) + PBMA (2) ($\bar{M}_n$ = 36 800 g/mol) at (□) 343.75, (○) 373.15, and (◇) 403.15 K compared to experimental data.[122] The solid lines correspond to the theoretical predictions.

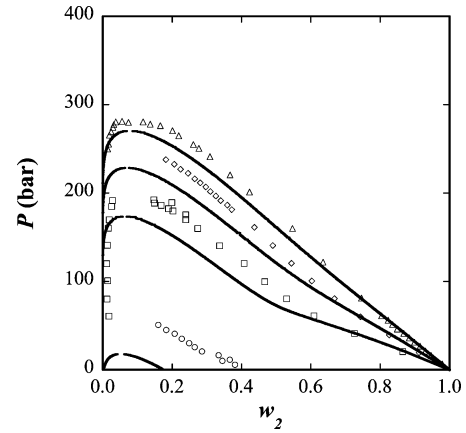

Figure 19. LLE of the binary mixture *n*-hexane (1) + LDPE (2) ($\bar{M}_n$ = 10 000 g/mol) at (○) 473, (□) 573, (◇) 623, and (Δ) 673 K from the GC-SAFT-VR approach compared to experimental data.[124] The solid lines correspond to theoretical predictions.

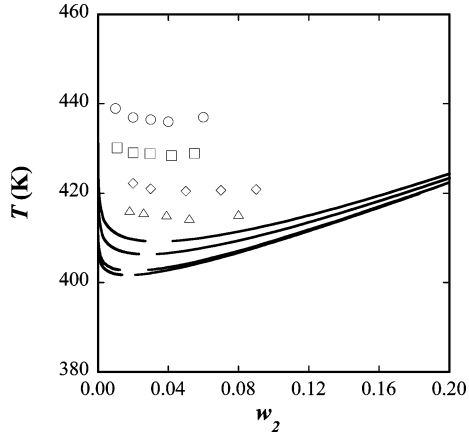

Figure 20. LLE predictions from the GC-SAFT-VR approach compared to experimental data[125] for the binary mixture diethyl ether (1) + PP (2) at 1 bar and $\bar{M}_w$ = (○) 18 100, (□) 28 700, (◇) 64 000, and (Δ) 83 500 g/mol.

Having shown that the vapor−liquid equilibria behavior of polymer systems is well captured by the GC-SAFT-VR approach, using no polymer mixture data to fit the functional group parameters or cross interactions, the performance of the GC-SAFT-VR EOS was further tested for binary polymer−solvent mixtures by considering liquid−liquid phase behavior. Liquid−liquid immiscibility of very asymmetric mixtures such as

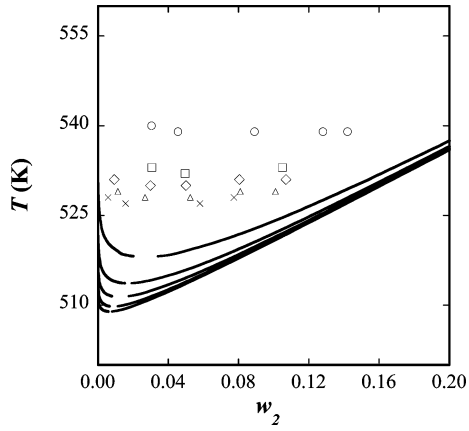

Figure 21. LLE predictions from the GC-SAFT-VR approach compared to experimental data[126] at 1 bar for the binary mixture benzene (1) + PS (2) at $\bar{M}_n$ = (○) 37 000, (□) 97 200, (◇) 200 000, (Δ) 400 000, and (×) 670 000 g/mol.

polymer systems are difficult to calculate, because the composition of polymer molecules in the solvent-rich phase can be very low. For this reason, several numerical methods have been reported in the literature.[45,110−114] We used the technique proposed by Paricaud[114] to find the coexisting compositions of the two liquid phases in which the spinodal compositions were obtained as a starting point for finding the binodals. Because the main focus of this work was the VLE behavior, here, we briefly present some examples of LLE for polymer systems in Figures 19−21. The LLE for low-density polyethylene (LDPE) with *n*-hexane ($\bar{M}_n$ = 10 000 g/mol) at different temperatures is shown in Figure 19. This system exhibits upper critical solution pressure (UCSP) behavior, where the region below each curve corresponds to the two-phase region. We found that, although the GC-SAFT-VR approach predicts the correct trend in phase behavior with varying temperature, it slightly underpredicts the experimental results. For the poly(polypropylene) (PP) + diethyl ether system presented in Figure 20, we found that lower critical solution temperature (LCST) behavior is observed, with the theory able to describe the decrease of the LCST as the molecular weight of the polymer is increased; however, the LLE curves are underpredicted. The same system was studied by Kouskoumvekaki et al.,[20] who presented LLE curves obtained from the PC-SAFT equation at same thermodynamic conditions using polymer parameters estimated from parameters for the *n*-alkane and fitted to polymer *PVT* data. We note that their results exhibited a larger underprediction of the LLE curves than seen with the GC-SAFT-VR approach, and a temperature-dependent binary interaction parameter was introduced to improve the agreement with experimental data. Finally, we considered mixtures of PS + benzene at 1 bar as shown in Figure 21. As can be seen in the figure, despite the increased complexity of the polymer molecule, the GC-SAFT-VR approach is again able to describe the LLE phase behavior of the system. Although the LCST and upper critical solution temperature (UCST) are underpredicted, the overall description of the liquid−liquid phase behavior is very good considering that the parameters used in the theoretical predictions were obtained from fitting to vapor pressure and saturated liquid density data of pure fluids and that no experimental data for polymer systems were needed.

Conclusions

In this work, the GC-SAFT-VR approach was applied to study the solubilities of a wide range of small molecules in polymer systems. The molecular parameters for the different functional groups in the polymer repeat units were obtained from the regression of experimental vapor pressure and saturated liquid density data for small molecules of several chemical families having the same functional groups as the polymers. The heterogeneity in the polymer structure (e.g., branching and functional groups) was then explicitly taken into account in the GC-SAFT-VR EOS through the retention of the functional groups in both the monomer and chain contributions. Overall, the GC-SAFT-VR EOS provides good predictions of the VLE behavior of several polymer systems

Table A1. Summary of Polymer Systems Considered

					ν_{pi}[a]											
polymer	figure(s)	$\bar{M}_w \times 10^{-3}$ [b]	$\bar{M}_n \times 10^{-3}$ [c]	n_u[d]	CH_2	CH_3	CH	CH_2—C	*cis*-CH=CH	C_6H_5	ether OCH_3	ether OCH_2	ether OCH	ester OCH	ester OCH_2	C=O
LDPE	4	76		2709	2											
LDPE	4		1.94	69	2											
LDPE	19		10	356	2											
PE	5		1.71	61	2											
PE	5		6.22	222	2											
poly(1-heptene)	6		224.1	2282	5	1	1									
poly(1-decene)	6		213.9	1525	8	1	1									
PBD	7	250		4622	2				1							
PS	8		53.7	516	1		1			1						
PS	9, 11, 12		290	2784	1		1			1						
PS	10		200	1920	1		1			1						
PS	21	37		355	1		1			1						
PS	21	97.2		933	1		1			1						
PS	21	200		1920	1		1			1						
PS	21	400		3841	1		1			1						
PS	21	670		6433	1		1			1						
PVME	13		14.6	251	1		1				1					
PVAc	14, 16		170	1975	1	1								1		1
PVAc	15		320	3717	1	1								1		1
PBMA	17, 18		36.8	259	2	2		1							1	1
PP	20		18.1	430	1	1	1									
PP	20		28.7	682	1	1	1									
PP	20		64	1521	1	1	1									
PP	20		83.5	1984	1	1	1									

[a] Number of functional groups of type *i* per polymer repeat unit. [b] Weight-average molecular weight. [c] Number-average molecular weight. [d] Number of repeat units within the polymer molecule.

containing different types of functional groups with parameters regressed from experimental data for pure components. For LLE, a good qualitative description of the phase behavior of polymer systems containing different types of functional groups was also achieved, considering that LLE is more sensitive to the molecular detail of the model. Furthermore, the effects of polymer molecular weight and branching on the VLE and LLE behavior of polymer solutions is accurately captured by the GC-SAFT-VR EOS. Deviations from Lorentz−Berthelot combining rules were seen in the phase behavior of systems with polymers and/or solvents containing a carbonyl (C═O) group with other groups including CH_2 and benzene. In these cases, the effects of the polar interactions were taken into account through the use of modified cross interactions determined from pure fluids or simple binary mixtures (in cases where the cross interactions were not present in a pure fluid). The modified cross interactions were found to be transferable to the study of other polymer−solvent systems involving the relevant functional groups. Recently, Zhao et al. developed the SAFT-VR+D equation to study dipolar chain fluids and explicitly take into account the location, magnitude, and orientation of dipolar interactions. We anticipate that, although the predictive capability of the GC-SAFT-VR approach is already impressive, the use of modified cross interactions could be eliminated or reduced if the polarity of the dipolar C═O functional group in the GC-SAFT-VR model were explicitly treated by combining the GC-SAFT-VR and SAFT-VR+D schemes.[73,115]

Acknowledgment

We gratefully acknowledge financial support from the National Science Foundation under Grant CTS-0452688 and an REU supplement to CTS-0452688. The authors also thank Jessica Haley for help with the collection of experimental data from the literature.

Appendix A

In Table A1, we present a summary of the polymer systems studied.

Literature Cited

(1) Bokis, C. P.; Orbey, H.; Chen, C. C. Properly model polymer processes. *Chem. Eng. Prog.* **1999**, *95* (4), 39–52.

(2) Zervopoulou, E.; Mavrantzas, V. G.; Theodorou, D. N. A new Monte Carlo simulation approach for the prediction of sorption equilibria of oligomers in polymer melts: Solubility of long alkanes in linear polyethylene. *J. Chem. Phys.* **2001**, *115* (6), 2860–2875.

(3) Economou, I. G. Statistical associating fluid theory: A successful model for the calculation of thermodynamic and phase equilibrium properties of complex fluid mixtures. *Ind. Eng. Chem. Res.* **2002**, *41* (5), 953–962.

(4) Lambert, S. M.; Song, Y.; Prausnitz, J. M. Equations of State for Polymer Systems. In *Equations of State for Fluids and Fluid Mixtures*, 1st ed.; Experimental Thermodynamics Series; Sengers, J. V., Kayser, R. F., Peters, C. J., White, H. J., Jr., Eds.; Elsevier: Amsterdam, 2000; Vol. V.

(5) Chapman, W. G.; Gubbins, K. E.; Jackson, G.; Radosz, M. SAFT: Equation-of-State Solution Model for Associating Fluids. *Fluid Phase Equilib.* **1989**, *52*, 31–38.

(6) Chapman, W. G.; Gubbins, K. E.; Jackson, G.; Radosz, M. New Reference Equation of State for Associating Liquids. *Ind. Eng. Chem. Res.* **1990**, *29* (8), 1709–1721.

(7) Müller, E. A.; Gubbins, K. E. Molecular-based equations of state for associating fluids: A review of SAFT and related approaches. *Ind. Eng. Chem. Res.* **2001**, *40* (10), 2193–2211.

(8) Muller, E. A.; Gubbins, K. E. Associating Fluids and Fluid Mixtures. In *Equations of State for Fluids and Fluid Mixtures*; Sengers, J. V., Kayser, R. F., Peters, C. J., White, H. J., Eds.; Elsevier: Amsterdam, 2001; Vol. 1.

(9) Huang, S. H.; Radosz, M. Equation of State for Small, Large, Polydisperse, and Associating Molecules. *Ind. Eng. Chem. Res.* **1990**, *29* (11), 2284–2294.

(10) Chen, C. A Segment-Based Local Composition Model for the Gibbs Energy of Polymer Solutions. *Fluid Phase Equilib.* **1993**, *83*, 301–312.

(11) Xiong, Y.; Kiran, E. Comparison of Sanchez−Lacombe and SAFT Model in Predicting Solubility of Polyethylene in High-Pressure Fluids. *J. Appl. Polym. Sci.* **1995**, *55* (13), 1805–1818.

(12) Orbey, H.; Bokis, C. P.; Chen, C. C. Equation of state modeling of phase equilibrium in the low-density polyethylene process: The Sanchez−Lacombe, statistical associating fluid theory, and polymer-Soave−Redlich−Kwong equations of state. *Ind. Eng. Chem. Res.* **1998**, *37* (11), 4481–4491.

(13) Jog, P. K.; Chapman, W. G.; Gupta, S. K.; Swindoll, R. D. Modeling of liquid−liquid-phase separation in linear low-density polyethylene−solvent system using the statistical associating fluid theory equation of state. *Ind. Eng. Chem. Res.* **2002**, *41* (5), 887–891.

(14) Wiesmet, V.; Weidner, E.; Behme, S.; Sadowski, G.; Arlt, W. Measurement and modelling of high-pressure phase equilibria in the systems polyethyleneglycol (PEG)−propane, PEG−nitrogen and PEG−carbon dioxide. *J. Supercrit. Fluids* **2000**, *17* (1), 1–12.

(15) ter Horst, M. H.; Behme, S.; Sadowski, G.; de Loos, T. W. The influence of supercritical gases on the phase behavior of polystyrene−cyclohexane and polyethylene−cyclohexane systems: Experimental results and modeling with the SAFT equation of state. *J. Supercrit. Fluids* **2002**, *23* (3), 181–194.

(16) Tumakaka, F.; Gross, J.; Sadowski, G. Modeling of polymer phase equilibria using perturbed-chain SAFT. *Fluid Phase Equilib.* **2002**, *194−197*, 541–551.

(17) Cheluget, E. L.; Bokis, C. P.; Wardhaugh, L.; Chen, C. C.; Fisher, J. Modeling polyethylene fractionation using the perturbed-chain statistical associating fluid theory equation of state. *Ind. Eng. Chem. Res.* **2002**, *41* (5), 968–988.

(18) Gross, J.; Sadowski, G. Modeling polymer systems using the perturbed-chain statistical associating fluid theory equation of state. *Ind. Eng. Chem. Res.* **2002**, *41* (5), 1084–1093.

(19) Kouskoumvekaki, I.; von Solms, N.; Michelsen, M. L.; Kontogeorgis, G. M. Application of the perturbed chain SAFT equation of state to complex polymer systems using simplified mixing rules. *Fluid Phase Equilib.* **2004**, *215*, 71–78.

(20) Kouskoumvekaki, I. A.; von Solms, N.; Lindvig, T.; Michelsen, M. L.; Kontogeorgis, G. M. Novel Method for Estimating Pure-Component Parameters for Polymers: Application to the PC-SAFT Equation of State. *Ind. Eng. Chem. Res.* **2004**, *43* (11), 2830–2838.

(21) von Solms, N.; Michelsen, M. L.; Kontogeorgis, G. M. Prediction and Correlation of High-Pressure Gas Solubility in Polymers with Simplified PC-SAFT. *Ind. Eng. Chem. Res.* **2005**, *44*, 3330–3335.

(22) McCabe, C.; Galindo, A.; Garcia-Lisbona, M. N.; Jackson, G. Examining the adsorption (vapor−liquid equilibria) of short- chain hydrocarbons in low-density polyethylene with the SAFT-VR approach. *Ind. Eng. Chem. Res.* **2001**, *40* (17), 3835–3842.

(23) Paricaud, P.; Galindo, A.; Jackson, G. Modelling the Cloud Curves and the Solubility of Gases in Amorphous and Semicrysttalline Polyethylene with the SAFT-VR Approach and Flory Theory of Crystallization. *Ind. Eng. Chem. Res.* **2004**, *43* (21), 6871–6889.

(24) Haslam, A. J.; von Solms, N.; Adjiman, C. S.; Galindo, A.; Jackson, G.; Paricaud, P.; Michelsen, M. L.; Kontogeorgis, G. M. Predicting enhanced absorption of light gases in polyethylene using simplified PC-SAFT and SAFT-VR. *Fluid Phase Equilib.* **2006**, *243* (1−2), 74–91.

(25) Dominik, A.; Chapman, W. G. Thermodynamic Model for Branched Polyolefins Using the PC-SAFT Equation of State. *Macromolecules* **2005**, *38*, 10836–10843.

(26) Arce, P.; Aznar, M. Modeling the phase behavior of commercial biodegradable polymers and copolymer in supercritical fluids. *Fluid Phase Equilib.* **2005**, *238* (2), 242–253.

(27) Pedrosa, N.; Vega, L. F.; Coutinho, J. A. P.; Marrucho, I. M. Phase Equilibria Calculations of Polyethylene Solutions from SAFT-Type Equations of State. *Macromolecules* **2006**, *39*, 4240–4246.

(28) Novak, A.; Bobak, M.; Kosek, J.; Banaszak, B. J.; Lo, D.; Widya, T.; Ray, W. H.; de Pablo, J. J. Ethylene and 1-hexene sorption in LLDPE under typical gas-phase reactor conditions: Experiments. *J. Appl. Polym. Sci.* **2006**, *100* (2), 1124–1136.

(29) von Solms, N.; Kouskoumvekaki, I. A.; Michelsen, M. L.; Kontogeorgis, G. M. Capabilities, limitations and challenges of a simplified PC-SAFT equation of state. *Fluid Phase Equilib.* **2006**, *241* (1−2), 344–353.

(30) Tihic, A.; Kontogeorgis, G. M.; von Sohns, N.; Michelsen, M. L.; Constantinou, L. A predictive group-contribution simplified PC-SAFT equation of state: Application to polymer systems. *Ind. Eng. Chem. Res.* **2008**, *47* (15), 5092–5101.

(31) Arce, P.; Aznar, M.; Mattedi, S. Fluid phase behavior modeling of CO_2 plus molten polymer systems using cubic and theoretically based equations of state. *Polym. Eng. Sci.* **2008**, *48* (6), 1157–1167.

(32) Tihic, A.; von Solms, N.; Michelsen, M. L.; Kontogeorgis, G. M.; Constantinou, L. Application of sPC-SAFT and group contribution sPC-SAFT to polymer systems—Capabilities and limitations. *Fluid Phase Equilib.* **2009**, *281* (1), 70–77.

(33) Lee, S. H.; Lostracco, M. A.; McHugh, M. A. High-Pressure, Molecular Weight-Dependent Behavior of (Co)Polymer−Solvent Mixtures: Experiments and Modeling. *Macromolecules* **1994**, *27* (17), 4652−4658.

(34) Banaszak, M.; Chen, C. K.; Radosz, M. Copolymer SAFT equation of state. Thermodynamic perturbation theory extended to heterobonded chains. *Macromolecules* **1996**, *29* (20), 6481–6486.

(35) Folie, B.; Gregg, C.; Luft, G.; Radosz, M. Phase equilibria of poly(ethylene-*co*-vinyl acetate) copolymers in subcritical and supercritical ethylene and ethylene−vinyl acetate mixtures. *Fluid Phase Equilib.* **1996**, *120* (1−2), 11–37.

(36) Pan, C.; Radosz, M. Copolymer SAFT modeling of phase behavior in hydrocarbon-chain solutions: Alkane oligomers, polyethylene, poly(ethylene-*co*-olefin-1), polystyrene, and poly(ethylene-*co*-styrene). *Ind. Eng. Chem. Res.* **1998**, *37* (8), 3169–3179.

(37) Shukla, K. P.; Chapman, W. G. TPT2 and SAFTD equations of state for mixtures of hard chain copolymers. *Mol. Phys.* **2000**, *98* (24), 2045–2052.

(38) Gross, J.; Spuhl, O.; Tumakaka, F.; Sadowski, G. Modeling Copolymer Systems Using the Perturbed-Chain SAFT Equation of State. *Ind. Eng. Chem. Res.* **2003**, *42* (6), 1266–1274.

(39) Becker, F.; Buback, M.; Latz, H.; Sadowski, G.; Tumakaka, F. Cloud-point curves of ethylene−(meth)acrylate copolymers in fluid ethene up to high pressures and temperatures—Experimental study and PC-SAFT modeling. *Fluid Phase Equilib.* **2004**, *215* (2), 263–282.

(40) Ghosh, A.; Blaesing, J.; Jog, P. K.; Chapman, W. G. Perturbed dipolar chains: A thermodynamic model for polar copolymers. *Macromolecules* **2005**, *38* (3), 1025–1027.

(41) Kleiner, M.; Tumakaka, F.; Sadowski, G.; Latz, H.; Buback, M. Phase equilibria in polydisperse and associating copolymer solutions: Poly(ethene-*co*-(meth)acrylic acid)−monomer mixtures. *Fluid Phase Equilib.* **2006**, *241*, 113–123.

(42) Arce, P.; Aznar, M. Modeling the thermodynamic behavior of poly(lactide-*co*-glycolide) plus supercritical fluid mixtures with equations of state. *Fluid Phase Equilib.* **2006**, *244* (1), 16–25.

(43) Tumakaka, F.; Sadowski, G.; Latz, H.; Buback, M. Cloud-point pressure curves of ethylene-based terpolymers in fluid ethene and in ethene−comonomer mixtures. Experimental study and modeling via PC-SAFT. *J. Supercrit. Fluids* **2007**, *41*, 461–471.

(44) Huang, S. H.; Radosz, M. Equation of State for Small, Large, Polydisperse, and Associating Molecules: Extension to Fluid Mixtures. *Ind. Eng. Chem. Res.* **1991**, *30* (8), 1994–2005.

(45) Chen, C. K.; Duran, M. A.; Radosz, M. Phase Equilibria in Polymer Solutions. Block-Algebra, Simultaneous Flash Algorithm Coupled with SAFT Equation of State, Applied to Single-Stage Supercritical Antisolvent Fractionation of Polyethylene. *Ind. Eng. Chem. Res.* **1993**, *32* (12), 3123–3127.

(46) Gross, J.; Sadowski, G. Application of perturbation theory to a hard-chain reference fluid: An equation of state for square-well chains. *Fluid Phase Equilib.* **2000**, *168* (2), 183–199.

(47) Gross, J.; Sadowski, G. Perturbed-chain SAFT: An equation of state based on a perturbation theory for chain molecules. *Ind. Eng. Chem. Res.* **2001**, *40* (4), 1244–1260.

(48) von Solms, N.; Michelsen, M. L.; Kontogeorgis, G. M. Applying association theories to polar fluids. *Ind. Eng. Chem. Res.* **2004**, *43* (7), 1803–1806.

(49) Gil Villegas, A.; Galindo, A.; Whitehead, P. J.; Mills, S. J.; Jackson, G.; Burgess, A. N. Statistical associating fluid theory for chain molecules with attractive potentials of variable range. *J. Chem. Phys.* **1997**, *106* (10), 4168–4186.

(50) Galindo, A.; Davies, L. A.; Gil-Villegas, A.; Jackson, G. The thermodynamics of mixtures and the corresponding mixing rules in the SAFT-VR approach for potentials of variable range. *Mol. Phys.* **1998**, *93* (2), 241–252.

(51) McCabe, C.; Galindo, A.; Gil-Villegas, A.; Jackson, G. Predicting the high-pressure phase equilibria of binary mixtures of *n*-alkanes using the SAFT-VR approach. *Int. J. Thermophys.* **1998**, *19* (6), 1511–1522.

(52) McCabe, C.; Gil-Villegas, A.; Jackson, G. Predicting the high-pressure phase equilibria of methane plus *n*-hexane using the SAFT-VR approach. *J. Phys. Chem. B* **1998**, *102* (21), 4183–4188.

(53) McCabe, C.; Jackson, G. SAFT-VR modelling of the phase equilibrium of long-chain *n*-alkanes. *PCCP Phys. Chem. Chem. Phys.* **1999**, *1* (9), 2057–2064.

(54) McCabe, C.; Kiselev, S. B. A crossover SAFT-VR equation of state for pure fluids: Preliminary results for light hydrocarbons. *Fluid Phase Equilib.* **2004**, *219* (1), 3–9.

(55) McCabe, C.; Kiselev, S. B. Application of crossover theory to the SAFT-VR equation of state: SAFT-VRX for pure fluids. *Ind. Eng. Chem. Res.* **2004**, *43* (11), 2839–2851.

(56) Galindo, A.; Florusse, L. J.; Peters, C. J. Prediction of phase equilibria for binary systems of hydrogen chloride with ethane, propane and *n*-dodecane. *Fluid Phase Equilib.* **1999**, *160*, 123–131.

(57) Filipe, E. J. M.; de Azevedo, E.; Martins, L. F. G.; Soares, V. A. M.; Calado, J. C. G.; McCabe, C.; Jackson, G. Thermodynamics of liquid mixtures of xenon with alkanes: (Xenon plus ethane) and (xenon plus propane). *J. Phys. Chem. B* **2000**, *104* (6), 1315–1321.

(58) Filipe, E. J. M.; Martins, L. F. G.; Calado, J. C. G.; McCabe, C.; Jackson, G. Thermodynamics of liquid mixtures of xenon with alkanes: (Xenon plus *n*-butane) and (xenon plus isobutane). *J. Phys. Chem. B* **2000**, *104* (6), 1322–1325.

(59) McCabe, C.; Dias, L. M. B.; Jackson, G.; Filipe, E. J. M. On the liquid mixtures of xenon, alkanes and perfluorinated compounds. *PCCP Phys. Chem. Chem. Phys.* **2001**, *3* (14), 2852–2855.

(60) Sun, L. X.; Zhao, H. G.; Kiselev, S. B.; McCabe, C. Application of SAFT-VRX to binary phase behaviour: Alkanes. *Fluid Phase Equilib.* **2005**, *228*, 275–282.

(61) Sun, L. X.; Zhao, H. G.; Kiselev, S. B.; McCabe, C. Predicting mixture phase equilibria and critical behavior using the SAFT-VRX approach. *J. Phys. Chem. B* **2005**, *109* (18), 9047–9058.

(62) Zhao, H. G.; Morgado, P.; McCabe, C.; Gil Villegas, A. Predicting the Phase Behavior of Nitrogen + *n*-Alkanes for Enhanced Oil Recovery from the SAFT-VR Approach: Examining the Effect of the Quadrupole Moment. *J. Phys. Chem. B* **2006**, *110* (47), 24083.

(63) Sun, L.; Zhao, H. G.; McCabe, C. Phase Equilibria of Gas Condensates and Light Petroleum Fractions from the SAFT-VR Approach. *AIChE J.* **2007**, *53* (3), 720–731.

(64) McCabe, C.; Galindo, A.; Gil-Villegas, A.; Jackson, G. Predicting the high-pressure phase equilibria of binary mixtures of perfluoro-*n*-alkanes plus *n*-alkanes using the SAFT-VR approach. *J. Phys. Chem. B* **1998**, *102* (41), 8060–8069.

(65) Morgado, P.; McCabe, C.; Filipe, E. J. M. Modelling the phase behaviour and excess properties of alkane plus perfluoroalkane binary mixtures with the SAFT-VR approach. *Fluid Phase Equilib.* **2005**, *228*, 389–393.

(66) Morgado, P.; Zhao, H. G.; Blas, F. J.; McCabe, C.; Rebelo, L. P. N.; Filipe, E. J. M. Liquid Phase Behavior of Perfluoroalkylalkane Surfactants. *J. Phys. Chem. B* **2007**, *111* (11), 2856–2863.

(67) Galindo, A.; Burton, S. J.; Jackson, G.; Visco, D. P.; Kofke, D. A. Improved models for the phase behaviour of hydrogen fluoride: Chain and ring aggregates in the SAFT approach and the AEOS model. *Mol. Phys.* **2002**, *100* (14), 2241–2259.

(68) Dias, L. M. B.; Bonifacio, R. P.; Filipe, E. J. M.; Calado, J. C. G.; McCabe, C.; Jackson, G. Liquid−vapour equilibrium of {$x$$BF_3$ + (1− x) *n*-butane} at 195.49 K. *Fluid Phase Equilib.* **2003**, *205* (1), 163–170.

(69) Dias, L. M. B.; Filipe, E. J. M.; McCabe, C.; Cordeiro, T.; Calado, J. C. G. Liquid mixtures of xenon with fluorinated species: Xenon plus sulfur hexafluoride. *J. Phys. Chem. B* **2007**, *111* (19), 5284–5289.

(70) Galindo, A.; Gil-Villegas, A.; Whitehead, P. J.; Jackson, G.; Burgess, A. N. Prediction of phase equilibria for refrigerant mixtures of difluoromethane (HFC-32), 1,1,1,2-tetrafluoroethane (HFC-134a), and pentafluoroethane (HFC-125a) using SAFT-VR. *J. Phys. Chem. B* **1998**, *102* (39), 7632–7639.

(71) McCabe, C.; Galindo, A.; Cummings, P. T. Anomalies in the solubility of alkanes in near-critical water. *J. Phys. Chem. B* **2003**, *107* (44), 12307–12314.

(72) Clark, G. N. I.; Haslam, A. J.; Galindo, A.; Jackson, G. Developing optimal Wertheim-like models of water for use in statistical associating fluid theory (SAFT) and related approaches. *Mol. Phys.* **2006**, *104* (22−24), 3561–3581.

(73) Zhao, H. G.; Ding, Y.; McCabe, C. Phase behavior of dipolar associating fluids from the SAFT-VR+D equation of state. *J. Chem. Phys.* **2007**, *127* (8), 4514.

(74) Galindo, A.; Blas, F. J. Theoretical examination of the global fluid phase behavior and critical phenomena in carbon dioxide plus *n*-alkane binary mixtures. *J. Phys. Chem. B* **2002**, *106* (17), 4503–4515.

(75) Colina, C. M.; Galindo, A.; Blas, F. J.; Gubbins, K. E. Phase behavior of carbon dioxide mixtures with *n*-alkanes and *n*-perfluoroalkanes. *Fluid Phase Equilib.* **2004**, *222*, 77–85.

(76) Colina, C. M.; Gubbins, K. E. Vapor−liquid and vapor−liquid−liquid equilibria of carbon dioxide/*n*-perfluoroalkane/*n*-alkane ternary mixtures. *J. Phys. Chem. B* **2005**, *109* (7), 2899–2910.

(77) dos Ramos, M. C.; Blas, F. J.; Galindo, A. Modelling the phase equilibria and excess properties of the water + carbon dioxide binary mixture. *Fluid Phase Equilib.* **2007**, *261*, 359–365.

(78) dos Ramos, M. C.; Blas, F. J.; Galindo, A. Phase equilibria, excess properties, and Henry's constants of the water plus carbon dioxide binary mixture. *J. Phys. Chem. C* **2007**, *111* (43), 15924–15934.

(79) Galindo, A.; Gil-Villegas, A.; Jackson, G.; Burgess, A. N. SAFT-VRE: Phase behavior of electrolyte solutions with the statistical associating fluid theory for potentials of variable range. *J. Phys. Chem. B* **1999**, *103* (46), 10272–10281.

(80) Gil-Villegas, A.; Galindo, A.; Jackson, G. A statistical associating fluid theory for electrolyte solutions (SAFT-VRE). *Mol. Phys.* **2001**, *99* (6), 531–546.

(81) Patel, B. H.; Paricaud, P.; Galindo, A.; Maitland, G. C. Prediction of the salting-out effect of strong electrolytes on water plus alkane solutions. *Ind. Eng. Chem. Res.* **2003**, *42* (16), 3809–3823.

(82) Zhao, H. G.; dos Ramos, M. C.; McCabe, C. Development of an Equation of State for Electrolyte Solutions by Combining the Statistical Associating Fluid Theory and the Mean Spherical Approximation for the Non Primitive Model. *J. Chem. Phys.* **2007**, *126* (24), 4503.

(83) Paricaud, P.; Galindo, A.; Jackson, G. Modeling the cloud curves and the solubility of gases in amorphous and semicrystalline polyethylene with the SAFT-VR approach and Flory theory of crystallization. *Ind. Eng. Chem. Res.* **2004**, *43* (21), 6871–6889.

(84) Adidharma, H.; Radosz, M. Prototype of an engineering equation of state for heterosegmented polymers. *Ind. Eng. Chem. Res.* **1998**, *37* (11), 4453–4462.

(85) Chen, S. J.; Economou, I. G.; Radosz, M. Density-Tuned Polyolefin Phase Equilibria. 2. Multicomponent Solutions of Alternating Poly(ethylene propylene) in Subcritical and Supercritical Olefins: Experiment and SAFT Model. *Macromolecules* **1992**, *25* (19), 4987–4995.

(86) Lymperiadis, A.; Adjiman, C. S.; Galindo, A.; Jackson, G. A group contribution method for associating chain molecules based on the statistical associating fluid theory (SAFT-γ). *J. Chem. Phys.* **2007**, *127*, 234903.

(87) Peng, Y.; Goff, K. D.; dos Ramos, M. C.; McCabe, C. Developing a predictive group-contribution-based SAFT-VR equation of state. *Fluid Phase Equilib.* **2009**, *277* (2), 131–144.

(88) Tamouza, S.; Passarello, J. P.; Tobaly, P.; de Hemptinne, J. C. Group contribution method with SAFT EOS applied to vapor liquid equilibria of various hydrocarbon series. *Fluid Phase Equilib.* **2004**, *222*, 67–76.

(89) Tamouza, S.; Passarello, J. P.; Tobaly, P.; de Hemptinne, J. C. Application to binary mixtures of a group contribution SAFT EOS (GC-SAFT). *Fluid Phase Equilib.* **2005**, *228*, 409–419.

(90) Thi, T. X. N.; Tamouza, S.; Tobaly, P.; Passarello, J. P.; de Hemptinne, J. C. Application of group contribution SAFT equation of state (GC-SAFT) to model phase behaviour of light and heavy esters. *Fluid Phase Equilib.* **2005**, *238* (2), 254–261.

(91) Le Thi, C.; Tamouza, S.; Passarello, J. P.; Tobaly, P.; de Hemptinne, J. C. Modeling phase equilibrium of H_2 + *n*-alkane and CO_2 + *n*-alkane binary mixtures using a group contribution statistical association fluid theory equation of state (GC-SAFT-EOS) with a k_{ij} group contribution method. *Ind. Eng. Chem. Res.* **2006**, *45* (20), 6803–6810.

(92) von Solms, N.; Michelsen, M. L.; Kontogeorgis, G. M. Computational and Physical Performance of a Modified PC-SAFT Equation of State for Highly Asymmetric and Associating Mixtures. *Ind. Eng. Chem. Res.* **2003**, *42* (5), 1098–1105.

(93) Lymperiadis, A.; Adjiman, C. S.; Jackson, G.; Galindo, A. A generalisation of the SAFT-γ group contribution method for groups comprising multiple spherical segments. *Fluid Phase Equilib.* **2008**, *274* (1−2), 85–104.

(94) Peng, Y.; Zhao, H. G.; McCabe, C. On the thermodynamics of diblock chain fluids from simulation and heteronuclear statistical associating fluid theory for potentials of variable range. *Mol. Phys.* **2006**, *104* (4), 571–586.

(95) Leonard, P. J.; Henderson, D.; Barker, J. A. Perturbation Theory and Liquid Mixtures. *Trans. Faraday Soc.* **1970**, *66* (574), 2439–2452.

(96) Boublik, T. Hard-Sphere Equation of State. *J. Chem. Phys.* **1970**, *53* (1), 471–472.

(97) Mansoori, G. A.; Carnahan, N. F.; Starling, K. E.; Leland, T. W. Equilibrium Thermodynamic Properties of Mixture of Hard Spheres. *J. Chem. Phys.* **1971**, *54* (4), 1523–1525.

(98) Patel, B. H.; Docherty, H.; Varga, S.; Galindo, A.; Maitland, G. C. Generalized equation of state for square-well potentials of variable range. *Mol. Phys.* **2005**, *103* (1), 129–139.

(99) Kirkpatrick, S.; Gelatt, C. D.; Vecchi, M. P. Optimization by Simulated Annealing. *Science* **1983**, *220* (4598), 671–680.

(100) Dolan, W. B.; Cummings, P. T.; Levan, M. D. Process Optimization via Simulated Annealing: Application to Network Design. *AIChE J.* **1989**, *35* (5), 725–736.

(101) Blei, I.; Odian, G. *General, Organic, and Biochemistry Media Update*, 2nd ed.; W. H. Freeman and Company: New York, 2009; p 800.

(102) Lafitte, T.; Bessieres, D.; Pineiro, M. M.; Daridon, J. L. Simultaneous estimation of phase behavior and second-derivative properties using the statistical associating fluid theory with variable range approach. *J. Chem. Phys.* **2006**, *124* (2), 16.

(103) dos Ramos, M. C.; Docherty, H.; Blas, F. J.; Galindo, A. Application of the generalised SAFT-VR approach for long-ranged square-well fuids to model the phase behaviour of real fuids. *Fluid Phase Equilib.* **2008**, *276*, 116.

(104) *NIST Chemistry WebBook*; NIST Standard Reference Database Number 69; National Institute of Standards and Technology (NIST): Gaithersburg, MD, 2005; available at http://webbook.nist.gov/chemistry/ (Accessed 2007).

(105) Paricaud, P.; Galindo, A.; Jackson, G. Modeling the Cloud Curves and the Solubility of Gases in Amorphous and Semicrystalline Polyethylene with the SAFT-VR Approach and Flory Theory of Crystallization. *Ind. Eng. Chem. Res.* **2004**, *43* (21), 6871–6889.

(106) Heuer, T.; Peuschel, G. P.; Ratzsch, M.; Wohlfarth, C. Investigations on Solubility of Ethene, Propane, Propene, and But-1-ene in Molten Oligomers of Polyethylene and Poly(ethene-*co*-vinyl acetate) at Temperatures up to 473.15 K and Pressures up to 30 MPa. 2. Model Calculations and Prediction. *Acta Polym.* **1989**, *40* (5), 320–324.

(107) Wohlfarth, C.; Finck, U.; Schultz, R.; Heuer, T. Investigation of Phase Equilibria in Mixtures Composed of Ethene, 1-Butene, 4-Methyl-1-Pentene and a Polyethylene Wax. *Angew. Makromol. Chem.* **1992**, *198*, 91–110.

(108) Haslam, A. J.; von Solms, N.; Adjiman, C. S.; Galindo, A.; Jackson, G.; Paricaud, P.; Michelsen, M. L.; Kontogeorgis, G. M. Predicting enhanced absorption of light gases in polyethylene using simplified PC-SAFT and SAFT-VR. *Fluid Phase Equilib.* **2006**, *243*, 74–91.

(109) NguyenHuynh, D.; Passarello, J. P.; Tobaly, P.; de Hemptinne, J. C. Application of GC-SAFT EOS to polar systems using a segment approach. *Fluid Phase Equilib.* **2008**, *264*, 62–75.

(110) Michelsen, M. L. The Isothermal Flash Problem. Part I. Stability. *Fluid Phase Equilib.* **1982**, *9* (1), 1–19.

(111) Michelsen, M. L. The Isothermal Flash Problem. Part II. Phase-Split Calculation. *Fluid Phase Equilib.* **1982**, *9* (1), 21–40.

(112) Michelsen, M. L. Calculation of Critical Points and Phase Boundaries in the Critical Region. *Fluid Phase Equilib.* **1984**, *16* (1), 57–76.

(113) Xu, G.; Brennecke, J. F.; Stadtherr, M. A. Reliable computation of phase stability and equilibrium from the SAFT equation of state. *Ind. Eng. Chem. Res.* **2002**, *41* (5), 938–952.

(114) Paricaud, P. Understanding the Fluid Phase Behaviour of Polymer Systems with the SAFT Theory. Ph.D. Thesis, Imperial College of London, London, 2003.

(115) Zhao, H. G.; McCabe, C. Phase Behavior of Dipolar Fluids from a Modified Statistical Associating Fluid Theory for Potentials of Variable Range. *J. Chem. Phys.* **2006**, *125* (10), 4504–4515.

(116) DIPPR 801 Database; Design Institute for Physical Property Data, American Institute of Chemical Engineers: New York, 1987.

(117) Semenov, A. A.; Suntsov, Y. K. Vapor−liquid equilibrium and thermodynamic properties of the system *n*-butylbenzene−benzene. Document deposited with VINITI, Moscow, Russia, 1998; N3709-V98, 10 pp.

(118) Linek, J.; Wichterle, I.; Polednova, J. Liquid−Vapor Equilibrium. LIII. The Systems Benzene−Diisopropyl Ether, Diisopropyl Ether−Toluene, Diisopropyl Ether−Ethylbenzene, Benzene−Dipropyl Ether, Dipropyl Ether−Toluene and Dipropyl Ether−Ethylbenzene. *Collect. Czech. Chem. Commun.* **1972**, *37*, 9.

(119) Treszczanowicz, T.; Lu, B. C. Y. Isothermal Vapor−Liquid−Equilibria for 11 Examples of (an Ether + a Hydrocarbon). *J. Chem. Thermodyn.* **1986**, *18* (3), 213–220.

(120) Nagata, I. Vapor−Liquid Equilibrium Data for Binary Systems, Acetone−Methyl Acetate, Methyl Acetate−Carbon Tetrachloride, Benzene−Butyl Acetate and Cyclohexane−Butyl Acetate. *Mem. Fac. Technol., Kanazawa Univ.* **1964**, *3*, 197–205.

(121) Surana, R. K.; Danner, R. P.; de Hann, A. B.; Beckers, N. New technique to measure high-pressure and high-temperature polymer−solvent vapour−liquid equilibrium. *Fluid Phase Equilib.* **1997**, *139*, 361–370.

(122) Wohlfarth, C. *Vapour−Liquid Equilibrium Data of Binary Polymer Solutions: Vapour Pressures, Henry Constants, And Segment Molar Excess Gibbs Free Energies*; Elsevier: Amsterdam, 1994.

(123) Hao, W.; Elbro, H. S.; Alessi, P. *Polymer Solution Data Collection*; DECHEMA: Frankfurt, 1992; Vol. XIV, Part 1.

(124) de Loos, T. W.; de Graaf, L. J.; de Swaan Arons, J. Liquid−Liquid Phase Separation In Linear Low Density Polyethylene−Solvent Systems. *Fluid Phase Equilib.* **1996**, *117*, 40–47.

(125) Cowie, J. M. G.; McEwen, I. J. Lower Critical Solution Temperatures of Polypropylene Solutions. *J. Polym. Sci. B: Polym. Phys.* **1974**, *12* (2), 441–443.

(126) Saeki, S.; Kuwahara, N.; Konno, S.; Kaneko, M. Upper and Lower Critical Solution Temperatures in Polystyrene Solutions. II. *Macromolecules* **1973**, *6* (4), 589–593.

(127) Hasch, B. M.; Lee, S. H.; McHugh, M. A. *J. Appl. Polym. Sci.* **1996**, *59*, 1107–1116.

Received for review May 15, 2009
Revised manuscript received September 22, 2009
Accepted November 19, 2009

IE900795X